

The dynamics of Domain Wall Strings

Jose J. Blanco-Pillado^{1,2,3*}, Daniel Jiménez-Aguilar^{1,2†},

Jose M. Queiruga^{4,5‡} and Jon Urrestilla^{1,2 §}

¹ *Department of Physics, University of Basque Country, UPV/EHU, 48080, Bilbao, Spain*

² *EHU Quantum Center, University of Basque Country, UPV/EHU*

³ *IKERBASQUE, Basque Foundation for Science, 48011, Bilbao, Spain*

⁴ *Department of Applied Mathematics,*

University of Salamanca, 37008, Salamanca, Spain

⁵ *Institute of Fundamental Physics and Mathematics,*

University of Salamanca, 37008 Salamanca, Spain.

Abstract

We study the dynamics of domain wall solitons in $(2 + 1)d$ field theories. These objects are extended along one of the spatial directions, so they also behave as strings; hence the name of domain wall strings. We show analytically and numerically that the amount of radiation from the propagation of wiggles on these objects is negligible except for regions of high curvature. Therefore, at low curvatures, the domain wall strings behave exactly as the Nambu-Goto action predicts. We show this explicitly with the use of several different numerical experiments of the evolution of these objects in a lattice. We then explore their dynamics in the presence of internal mode excitations. We do this again by performing field theory simulations and identify an effective action that captures the relevant interactions between the different degrees of freedom living on the string. We uncover a new parametric resonance instability that transfers energy from the internal mode to the position of the domain wall. We show that this instability accelerates the radiation of the internal mode energy. We also explore the possibility of exciting the internal mode of the soliton with the collision of wiggles on the domain wall. Our numerical experiments indicate that this does not happen unless the wiggles have already a wavelength of the order of the string thickness. Finally, we comment on the possible relevance of our findings to cosmological networks of defects. We argue that our results cast some doubts on the significance of the internal modes in cosmological applications beyond a brief transient period right after their formation. This, however, should be further investigated using cosmological simulations of our model.

* josejuan.blanco@ehu.eus

† daniel.jimenez@ehu.eus

‡ xose.queiruga@usal.es

§ jon.urrestilla@ehu.eus

I. INTRODUCTION

Solitons emerge as non-perturbative solutions of field theory models in many branches of physics from condensed matter to particle physics or cosmology. In many cases, these solitons are created at a symmetry breaking phase transition. The energy scale associated with this transition is therefore the characteristic scale of the problem when studying these objects. Their mass as well as their size is controlled by this scale. This also suggests that the typical excitations of these solutions should relax to the lowest energy configuration on a time of the order of the characteristic scale of the soliton, the light crossing time of the object. All this seems to indicate that if we are only interested in studying these objects at low energies or for long periods of time, we can forget about these excitations.

However, the study of field theory perturbations around these stable solutions reveals that in many cases there are long lived excitations spatially localized around the soliton [1–5]. This extra energy gives rise to a new kind of object, the excited soliton, whose macroscopic behaviour could be altered by the presence of these excitations. Furthermore, the existence of these localized modes points to an interesting coupling of the soliton to the radiation modes. This coupling enables the soliton to slowly relax to the lowest energy configuration but also indicates the possibility of interactions with the environment. All these processes could in principle become important in the study of the dynamics of these objects.

On the other hand, depending on the particular model and the dimensionality of space-time, these solitons could appear as extended objects such as strings or domain walls in $(3 + 1)$ dimensions. The presence of these longitudinal directions allows for possible excitations of the soliton to propagate along them. For a particular model there could be more than one type of these excitations. For example, in some models one could have waves of the localized modes described earlier travelling along the objects. In addition, the breaking of translational invariance by the object guarantees the appearance of Goldstone modes living on the worldvolume of these solitons. In general, one would have perturbations of all these modes moving up and down the soliton, interacting among themselves and possibly emitting or absorbing radiation. It is therefore clear that in order to understand the dynamics of these objects one would need to find the conditions when these excitations become important and obtain the effective theory that governs these modes and their interactions.

A traditional approach to this problem has used the fact that there is a separation of scales between the different sets of perturbations present in these objects. The localized excitations on the core of the solitons have typically masses comparable with the characteristic scale of the field theory that gives rise to them. However, the perturbations that represent wiggles on the solitons are, by definition, massless from the point of view of the effective theory living on the worldvolume. Therefore, a reasonable strategy to find an approximate description

of the soliton’s dynamics would be to identify the action that captures the interactions of the low energy degrees of freedom, in this case, the massless modes. This assumes that the massive modes are not easily excited by the subsequent evolution since the energy required to excite them is not present at late times.

In the case of strings, this approach leads to the use of the so-called Nambu-Goto (NG) action [6–8]. This action is basically the generalization to the case of a string of the relativistic particle action and it is described by the area of the worldsheet of the string ¹. Taking this viewpoint, one can develop large scale simulations that track the motion of a network of strings. This is particularly interesting in the context of cosmology, where these relativistic strings have been predicted in many extensions of the Standard Model [9, 10].

Alternatively, one can simulate the dynamics of these objects evolving the full field theory in a lattice. This method follows all the degrees of freedom and in principle one includes all the interactions between them. However, the obvious price to pay in this case is the limited dynamic range that one can have in these simulations. Resolving all the field theory structure in the solitons at scales smaller than their thickness means that one can not simulate as many strings as in the Nambu-Goto case.

It has always been assumed that both methods should be reconciled in some regime demonstrating their complementarity to study the dynamics of these strings. However, some of the results from field theory simulations of local cosmic string networks deviate from their NG counterparts. In particular, these lattice simulations seem to indicate that loops (closed strings) produced during their cosmological evolution quickly collapse and disappear. This is in contrast with the results in NG dynamics, where one is expected to have some long lived oscillating loops. This apparent mismatch between both types of simulations is even more puzzling taking into account that simulations of individual strings in field theory do indeed follow the NG dynamics [11, 12]. Understanding this puzzling issue has become one of the central problems in the cosmic string community, specially since it is of paramount importance in the calculation of the expected gravitational wave signatures of these models [13, 14].

Recently, it has been suggested that this different behaviour of string loops could be due to the presence of excited strings in the field theory simulations [15, 16]. Moreover, it was also conjectured that these excitations could be in the form of localized bound modes on the strings that we mentioned earlier. This argues for a possible extension of the effective theory of the string motion by including these extra massive modes. Exploring this possibility in detail in a realistic $(3+1)$ dimensional simulation is quite difficult, so here we will investigate

¹ Note that this is also an approximation on the more general action that would include corrections due to the thickness of the string.

this issue in a simpler setting, in $(2 + 1)d$. Even though the problem that we study in the present paper is quite different from the actual situation for strings, it shares many of the issues that are at play in that case. We will study domain wall solitons that in $(2 + 1)$ dimensions behave as string-like objects, thus the name *domain wall strings* in our title. Their effective action within the thin wall approximation is identical to the Nambu-Goto action for strings. Furthermore, we will demonstrate that the walls in these simple scalar field models have bound state excitations stuck to their core that decay slowly into radiation. Therefore, the lower dimensional problem that we will study here has all the ingredients that have been presented in the hypothetical resolution of the local cosmic string puzzle. Taking all this into account, we hope that some of our results and conclusions can be extrapolated to the actual problem with local strings.

The organization of the paper is the following. In Section II we will describe the field theory model that gives rise to the domain wall solutions that we are interested in studying and discuss the different types of fluctuations that one can obtain around these solutions. In section III we will discuss the different processes that lead to energy loss by the domain wall dynamics. In Section IV we discuss the dynamics of these domain wall strings in the absence of any internal excitation, paying particular attention to the region of validity of the thin wall approximation, the Nambu-Goto equations of motion. In Section V we include the presence of massive excitations on the effective action and discuss their possible dynamical implications. In Section VI we explore the non-linear interactions between the excitations on the string and their Goldstone modes. We demonstrate the existence of resonance effects between them and the transfer of energy between these modes as well as their radiation. In Section VII we study the possible generation of the bound state mode from the interaction of Goldstone modes. Finally, we summarize our results in the conclusions and give a brief description of the relevance of these effects for cosmological networks.

Some examples of the simulations we have performed in this paper can be found at <http://tp.lc.ehu.es/earlyuniverse/dynamics-of-domain-wall-strings>.

II. FIELD THEORY MODEL FOR DOMAIN WALLS AND THEIR EXCITATIONS

The field theory model that we will investigate in this paper is described by the following $(2 + 1)$ dimensional action for a scalar field $\phi(x, y, t)$:

$$S = \int d^3x \left[\frac{1}{2} \partial_\mu \phi \partial^\mu \phi - \frac{\lambda}{4} (\phi^2 - \eta^2)^2 \right], \quad (1)$$

whose equations of motion are therefore given by

$$\partial_\mu \partial^\mu \phi + \lambda \phi (\phi^2 - \eta^2) = 0 . \quad (2)$$

Looking at this equation, one can immediately identify the existence in this theory of two degenerate vacua at $\phi = \pm\eta$. Small fluctuations about each of these vacua give rise to the perturbative excitations of the theory, whose masses are given by $m^2 = 2\lambda\eta^2$. In other words, the theory we will consider has a gap since there are no massless propagating modes in the $2+1$ dimensional vacua of this theory. This is important for our considerations since, as will discuss later on, this will be the only available channel for decay of any excitation present on the solitons. This, in turn, will determine the different time scales associated with those excitations.

A. The domain wall string solution

It is well known that this theory possesses, as part of its spectrum, non-perturbative solitonic solutions that interpolate between the two vacua. These solitons can easily be obtained as static solutions of the equations of motion of the theory and take the following functional form:

$$\phi_K(x, y, t) = \eta \tanh\left(\frac{m}{2}x\right) . \quad (3)$$

The properties of these solutions are well known and have been studied in many papers before (see for example the review in [17]). Here we will briefly summarize the most important results relevant for the rest of our discussion.

The first important result is about stability. One can show that these configurations are stable once one imposes the asymptotic boundary conditions for $x \rightarrow \pm\infty$. This property is inherited from the analogue solution of the $1+1$ theory, the kink solution, and represents the prototypical example of topological stability².

Furthermore, the configuration in Eq. (3) does not depend on one of the coordinates, in our case the y direction. This means that one should think about this soliton as an extended object along that direction. It is easy to check that most of the energy density on these field solutions is concentrated within a narrow area of thickness $\delta \sim m^{-1}$ around the $\phi = 0$ region (the core). Taking this into account, we can consider this object as a line-like defect in our lower dimensional spacetime in $(2+1)$ d. This means that even though these field

² This does not mean that all configurations constructed with these solutions are stable. In $2+1$ dimensions one can easily build configurations, like a circular loop of the kink soliton, that will be unstable to collapse. We will discuss both types of solutions in our paper.

configurations are domain walls that separate two different vacua in our model they will dynamically behave as strings. That is why we named them *domain wall strings*.

Finally, given the solution we can compute the equation of state associated to these string-like objects. Given the fact that these field configurations are independent of the y direction as well as time, we can see that these domain wall strings will have a relativistic string equation of state where the energy per unit length is equal to the pressure along the y direction, the tension of the string. One can compute this energy per unit length analytically in our model and find that ³

$$\mu = \left(\frac{m}{3\lambda}\right) m^2 . \quad (4)$$

B. Spectrum of excitations

We can now study the spectrum of small perturbations around the static solution given by Eq. (3). In order to do this, we will start by considering the following ansatz for these perturbations ⁴:

$$\phi(x, y, t) = \phi_K(x) + f_n(x)e^{i(k_n y - \omega_n t)} . \quad (5)$$

Inserting this expression in the equations of motion for the scalar field we obtain, at the linear level, the following equations:

$$-f_n''(x) + U(x)f_n(x) = \Omega_n^2 f_n(x) , \quad (6)$$

where

$$U(x) = \lambda (3\phi_K^2(x) - \eta^2) \quad (7)$$

is the effective potential for this Schrödinger problem and the associated eigenvalues are described in terms of the parameters in the ansatz as

$$\Omega_n^2 = \omega_n^2 - k_n^2 . \quad (8)$$

It turns out that the eigenvalue problem given by Eq. (6) can be exactly solved [18]. Its spectrum is given in terms of two bound states whose properly normalized eigenfunctions are

$$f_0(x) = \sqrt{\frac{3m}{8}} \operatorname{sech}^2\left(\frac{mx}{2}\right) \quad \text{with} \quad \Omega_0 = 0 \quad (9)$$

and

$$f_1(x) = \sqrt{\frac{3m}{4}} \sinh\left(\frac{mx}{2}\right) \operatorname{sech}^2\left(\frac{mx}{2}\right) \quad \text{with} \quad \Omega_1 = \frac{\sqrt{3}}{2}m , \quad (10)$$

³ Note that in 2 + 1 dimensions the parameter λ has units of energy.

⁴ Here we closely follow the discussion given in [4], where the study of this spectrum was done in a lower dimensional setup.

and a continuum of states starting at $\Omega_n = m$.

Each of these modes has a simple physical interpretation which follows from their lower dimensional analogues [4]. The modes characterised by $\Omega_0 = 0$ represent the local rigid displacements of the domain wall profile that propagate at the speed of light along the longitudinal directions of the object, the homogeneous one being just a rigid displacement of the whole object.

The modes associated with the other bound state, with $\Omega_1 = \frac{\sqrt{3}}{2}m$, represent travelling excitations of the so-called *internal mode* or *shape mode*. One can think of it as a perturbation in the width of the soliton that oscillates in time with frequency Ω_1 .

The profiles of the zero mode and the shape mode, given respectively in Eqs. (9) and (10), are shown in Fig. 1. We note that both these modes have a spatial extent comparable to the size of the soliton itself, namely, $\delta \sim m^{-1}$.

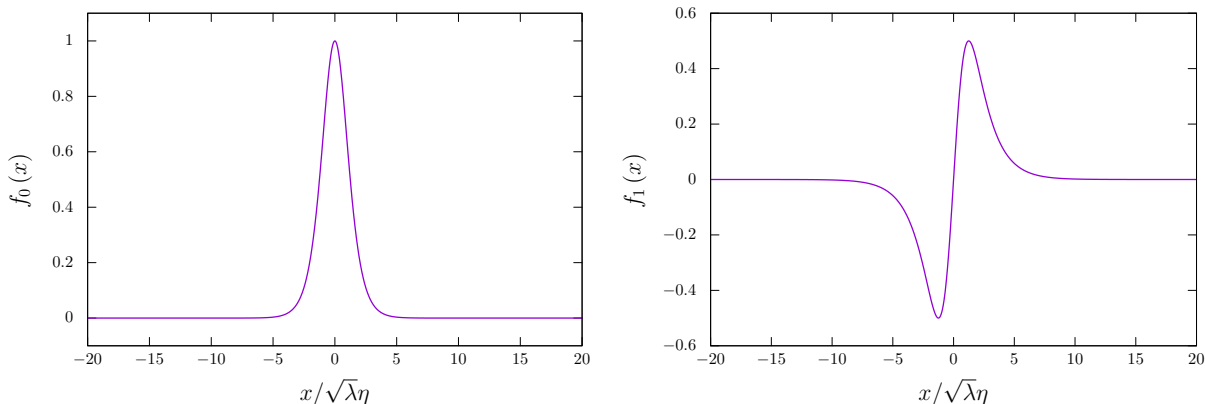


FIG. 1: Zero mode (left panel) and shape mode (right panel) excitations.

Finally, there is also the continuum of scattering modes starting at frequency m that represent all the excitations of the field outside of the soliton; in the vacuum. A generic field configuration would be described as a combination of all these modes with their corresponding amplitude. In the following, we will try to understand how to describe the dynamics of the domain wall string in the presence of some of these perturbations and their possible interactions.

III. RADIATION FROM DOMAIN WALL EXCITATIONS

As we described in the introduction, one of our goals is to identify the appropriate dynamics that characterises the domain wall string motion and its coupling to the internal modes. This task would be greatly simplified if we could write an effective action for all the modes populating the string in a $2d$ worldsheet theory. However, this type of action disregards the

possibility of energy leaking into the bulk, so in order to be able to quantify the regime of validity of this approach, one should understand the presence of radiative processes first.

A. Radiation from zero mode excitations

As we alluded earlier, the zero mode excitations represent the Goldstone modes associated with the wiggles of the domain wall string. A very interesting result due to Vachaspati and Vachaspati [19] shows that one can obtain the fully non-linear description of these excitations at the field theory level. In particular, assuming a domain wall extended along the y direction, one can show that the configuration of the form

$$\phi(x, y, t) = \phi_K(x - \psi(y \pm t)) \quad (11)$$

is an exact solution of the domain wall field theory with an arbitrary transverse excitation of the form $\psi(y \pm t)$. This wiggle moves at the speed of light in one direction along the domain wall and does not change its shape. The energy is conserved, so no radiation is being emitted from these waves. However, the most general configuration of the zero mode excitations will have in general fluctuations propagating in both directions. In this case, we expect some radiation to be emitted from the domain wall.

In order to study this radiation in a quantitative manner, we will start by investigating the energy loss from a particular set of perturbations described by standing waves where the center of the domain wall is parametrized by

$$\psi_0(y, t) = \hat{D} \cos(\omega_0 y) \cos(\omega_0 t) . \quad (12)$$

A configuration of this type is not an exact solution. However, for small enough amplitude, we expect these waves to behave like a free field on the worldsheet, as the linear theory predicts. Their oscillation will then act as a source for radiation at a quadratic order in their amplitude. It is this radiation that we want to study.

We compute in the Appendix C 1 the approximated power emitted per unit length of the domain wall string from these configurations as a function of the frequency ω_0 . In order to perform this calculation we have assumed that the scalar field profile during these oscillations is well approximated by the ansatz

$$\phi(x, y, t) = \phi_K \left(\frac{x - \psi_0(y, t)}{\sqrt{1 - \partial_a \psi_0 \partial^a \psi_0}} \right) , \quad (13)$$

where $a = (y, t)$ are the coordinates on the worldsheet of the domain wall string. We demonstrate in the Appendix B that this ansatz is a good approximation for the full field

theory equations as long as the second derivatives of the function $\psi(y, t)$ are small ⁵.

On the other hand, we have also explored this process in a field theory lattice simulation. Taking the ansatz given above, we can initialize the numerical simulations for a sinusoid excitation of a particular wavelength and amplitude:

$$\phi(x, y, 0) = \phi_K \left(\frac{x - \hat{D} \cos(\omega_0 y)}{\sqrt{1 + \hat{D}^2 \omega_0^2 \sin^2(\omega_0 y)}} \right), \quad \dot{\phi}(x, y, 0) = 0. \quad (15)$$

This initial state has the form shown in Fig. 2.

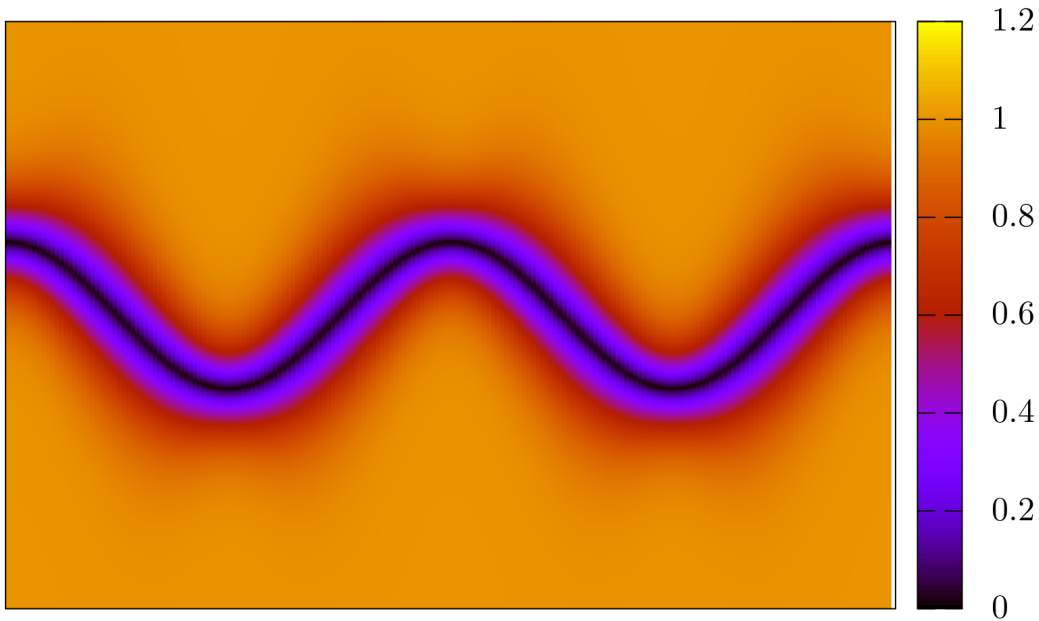


FIG. 2: Initial configuration (15). The color palette indicates the value of $|\phi|/\eta$.

Evolving this configuration in a box with absorbing boundary conditions on the boundaries transverse to the string, we can obtain the power emitted at each moment in time directly from the simulation ⁶. We can actually do this in two different ways: either by look-

⁵ As we note in the Appendix B, this ansatz for the field profile is the correct one for a string moving according to the Nambu-Goto action as we expect for these types of waves. We will have much more to say about this expectation in the coming sections on the validity of the Nambu-Goto action later on in the paper. We could have also taken the ansatz

$$\phi(x, y, t) = \phi_K(x) + \psi_0(y, t) \times f_0(x), \quad (14)$$

which is the linear approximation of the one we used. The results in this case are qualitatively similar to the ones presented here.

⁶ See the details of the field theory techniques that we use throughout this paper in Appendix A.

ing at the decrease of the total energy in the box or by integrating the energy flux through a surface near the boundary. Both strategies yield consistent results.

We show in Fig. 3 the comparison of this power computed using the analytic expression and the numerical simulations. The results show a very good agreement between these two approaches.

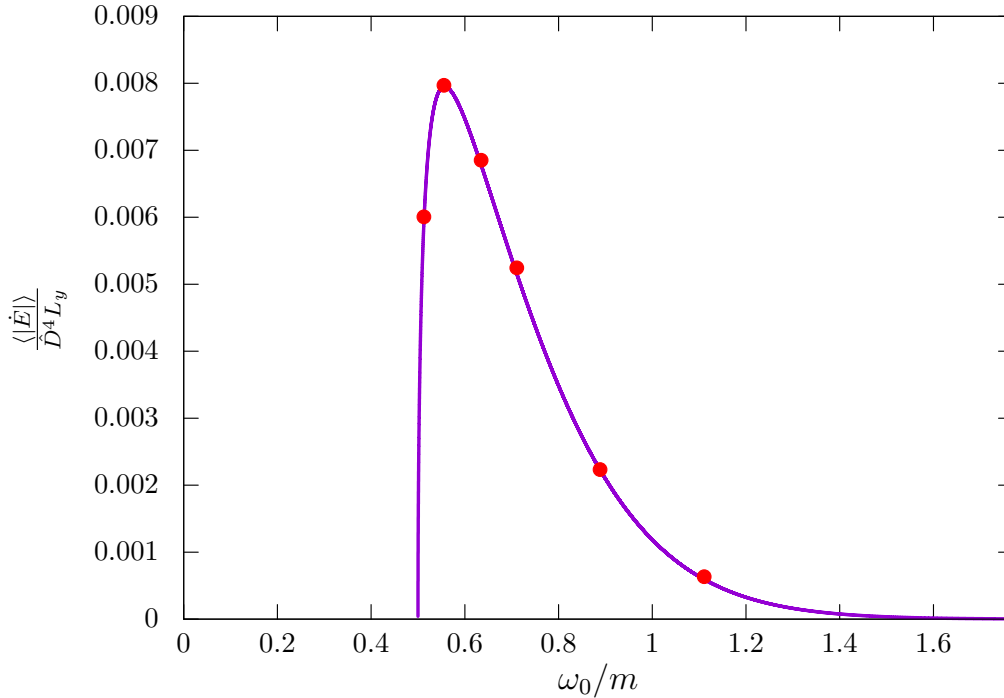


FIG. 3: Radiated power per unit length as a function of the frequency of the zero mode. The quantity on the y axis is made dimensionless by dividing the power by $\lambda^3 \eta^8$. The solid curve corresponds to the analytical estimate (C6), and the red points represent the power read directly from the numerical simulations.

These results indicate several important facts for us. First and foremost, it is clear that for a frequency below $\omega_* = \frac{m}{2}$, the radiation is highly suppressed. In fact, it is easy to see in the analytic calculation that the quadratic order coupling shuts off at frequencies below this threshold value. This can be easily understood by recognizing that below this frequency the quadratic source would oscillate with a frequency below the lowest propagating mode in the vacuum. This indicates that for low amplitudes and for frequencies below ω_* one should not expect any appreciable radiation ⁷.

Increasing the frequency of oscillation beyond this threshold, the string starts radiating

⁷ This is, of course, not strictly true since there should be some higher order radiation. However, at low enough frequencies, this should be negligible since the radiation would be quartic on the amplitude.

slowly and its power grows with frequency. However, this will also shut down for high enough frequency. This effect is basically due to the finite size of the source, which in our model is also parametrized by the mass of the particle being radiated (m). This peculiar behaviour is due to the fact that both scales, the mass of the particle radiated and the inverse of the size of the source, are of the same order.

We can also take this type of ansatz and extend it beyond its range of expected validity to study waves of high amplitude and curvature. In this case, a new source of radiation appears that has to do with the regions of high curvature. The standing wave solutions we are discussing will have their highest curvature at their maximum extension. We have observed that these configurations seem to radiate much more intensively in the case where the associated radius of curvature is of the order of the domain wall thickness. This is not surprising since in this case we expect the different segments of the string to start interfering with one another since they are forced to be closer than their own thickness. This is reminiscent to what happens at the high curvature regions in the case of local cosmic strings [11, 12].

In Fig. 4 we illustrate how the standing wave loses energy in the form of non-perturbative radiation. We choose an angular frequency below $m/2$ so that the zero mode does not couple quadratically to the scattering states, and look at the power emitted by the standing wave as we gradually increase its amplitude. We see that for low amplitudes the radiation is negligible and it is enhanced for large amplitudes.

We can also describe the different configurations by specifying their ratio between the domain wall string thickness and the radius of curvature at the crests of the waves, namely the quantity

$$\kappa = \frac{\delta}{(\hat{D}\omega_0^2)^{-1}}. \quad (16)$$

We note that the radiated power is only significant for large amplitudes where $\kappa \geq 0.5$. This seems to be in agreement with the expectations that this energy loss mechanism has a non-perturbative origin.

B. Radiation from internal mode excitations

As we described before, a homogeneous internal excitation on the domain wall (one that is independent of the y coordinate) would lead to an oscillation of the soliton thickness⁸ with a frequency such that $2\Omega_1 > m$. This tells us that non-linear effects will lead to radiation

⁸ One can see this by looking at the profile of the internal mode given in Fig. 1.

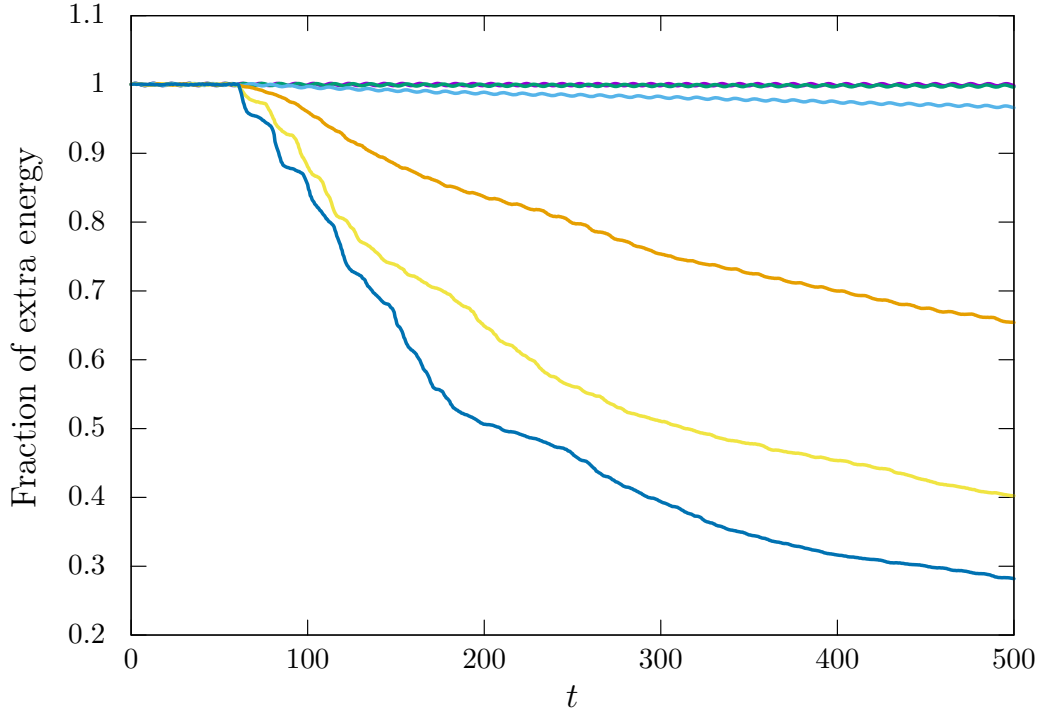


FIG. 4: Fraction of extra energy as a function of time, given in units of $(\sqrt{\lambda\eta})^{-1}$, for standing waves with increasing amplitudes. “Extra energy” means total energy inside the box minus energy of the straight domain wall. From top to bottom, the amplitudes of the standing waves are $\hat{D} = 0.5, 1, 2, 4, 6$, and 8 , with corresponding curvatures (i.e., ratio of string thickness to radius of curvature) $\kappa = 0.07, 0.14, 0.28, 0.56, 0.84$, and 1.12 . In all cases, the frequency of the standing wave is $\omega_0 < m/2$.

since these excitations can act as a source of modes that are allowed to propagate in the bulk.

This effect was extensively studied in numerical simulations in $1 + 1$ dimensions in [4] for kinks excited with the internal or shape mode. Here we will just outline the most important findings of that paper.

Assuming that one starts with a homogeneous excitation of the bound state of the form

$$\phi(x, y, t) = \phi_K(x) + \hat{A}(t) \cos(\Omega_1 t) \times f_1(x) , \quad (17)$$

one can show [4, 20] that its amplitude will follow a time dependent expression of the form

$$\hat{A}(t)^{-2} = \hat{A}(0)^{-2} \left(1 + \frac{t}{\tau} \right) , \quad (18)$$

where

$$\tau = \left(\frac{\Gamma}{\hat{A}(0)^2} \right) m^{-1} . \quad (19)$$

Γ is a numerical coefficient that can be analytically computed from the kink profile and is of $\mathcal{O}(100)$. This expression demonstrates that the shape mode amplitude decreases slowly compared to the time scale associated with the thickness of the soliton. This justifies the interest on the amplitude of these modes in field theory simulations, which can be running for a short time compared to this decay time.

The physical reason for this slow decay of the shape mode can be traced back to its non-linear origin. At the linear level the shape mode is stable, but with the non-linear interactions included, one can see the presence of radiation that slowly depletes the energy of this mode. This was shown to be the case explicitly in simulations performed in [4].

We can also look at the evolution of more complicated configurations where the shape mode is excited in the form of a standing wave with some finite wavelength along the y direction. The analytic estimates presented in Appendix C 2 show that for frequencies not too large compared to the mass of the propagating particle in the bulk, the associated decay time scale for these modes is comparable to the homogeneous one ⁹.

Finally, similarly to what happens in the case of the zero modes, we should always keep in mind that these results are accurate when one considers small amplitude perturbations. Going beyond this will introduce errors that could lead to drastically different evolutions of the field. This, for example, limits the amplitude of the homogenous shape mode to be below unity. At high amplitudes, the soliton will not be able to sustain the excitation and can lead to pair creation of solitons [4]¹⁰.

All these considerations suggest that we could try to write an effective action for the excited domain walls for small curvatures and time scales $t < \tau$. In this regime, the amount of radiation from the domain wall should be sub-dominant and one could try to find the relevant couplings between the different modes on the worldsheet. That action would allow us to explore the mechanical backreaction on the domain walls due to the presence of the shape mode. This could lead to different dynamics of the domain walls and perhaps explain the different behaviour of strings in field theory simulations. However, before we do that, let's start by identifying in the next section the correct action in the absence of any internal excitation. After that, we will add new terms to the action that capture the new dynamics and couplings between the zero and internal modes.

⁹ We can also think about travelling waves of this mode moving in one direction. However, these configurations can be brought to look like the homogeneous one by a boost along the longitudinal direction of the domain wall. Therefore, we could estimate the new time scale associated to their decay by performing this boost on the homogeneous mode.

¹⁰ You can also look at the simulations in <http://tp.lc.ehu.es/earlyuniverse/kink-simulations>

IV. THE DYNAMICS OF BARE DOMAIN WALL STRINGS

Let's consider for a moment the low energy dynamics of our domain walls in $(2+1)d$. At these low energies the internal mode will not get excited, so one can assume that the only dynamical degree of freedom is the position of the wall. Furthermore, we will also assume that there are no high curvature regions excited on the domain wall, so we can neglect the effects of radiation.

The evolution of the wall can then be described by a $2d$ worldsheet specified by the 3-vector $X^\mu(\xi^0, \xi^1)$, where ξ^a are the internal coordinates of the worldsheet with $(a = 0, 1)$. The simplest possible action describing the dynamics of these objects can be found by generalizing the relativistic point particle action to a line-like object. Following this idea, we conclude that the action of a relativistic string-like object should be identified with the area of its worldsheet, namely,

$$S_{NG} = -\mu \int d^2\xi \sqrt{-\gamma}, \quad (20)$$

where γ denotes the determinant of the induced metric on the worldsheet and μ is the energy per unit length of the object. This is the so-called Nambu-Goto action [6–8].

It is clear that this action is invariant under reparametrizations of the worldsheet coordinates. This is good since it means that the physics does not depend on the way we choose our coordinate system on the domain wall string worldsheet. This also means that there are many different gauges that one can adopt to describe the dynamics of the wall. The equations of motion in any gauge are given by

$$\partial_a (\sqrt{-\gamma} \gamma^{ab} X_{,b}^\mu) = 0, \quad (21)$$

where the induced metric is given by

$$\gamma_{ab} = \eta_{\mu\nu} \partial_a X^\mu \partial_b X^\nu. \quad (22)$$

Our goal in this section of the paper is to compare the evolution of the field theory solitons in $2+1$ dimensions we presented earlier with the solutions predicted by these equations. In order to do that, we will design several numerical experiments that will allow us to understand the physical conditions that should be met for these two descriptions of the same physics to agree.

The equations of motion for the Nambu-Goto string wall written above look quite complicated. In particular, expanding them in terms of our variables, the functions X^μ , we would obtain a scary-looking set of non-linear differential equations. We could, of course, solve them numerically as well. However, the situation is greatly simplified by a judicious choice of gauge.

Let us start our discussion with the usual conformal gauge¹¹. In this case, one identifies the timelike coordinate with the zero component of the string position, $X^0 = t$, and uses the gauge freedom to impose the following conditions on the 2-vector \mathbf{X} that denotes the position of the string:

$$\dot{\mathbf{X}} \cdot \mathbf{X}' = 0 , \quad (23)$$

$$\dot{\mathbf{X}}^2 + \mathbf{X}'^2 = 1 . \quad (24)$$

Here, and in the rest of the paper, the derivatives with respect to time are denoted by a dot and the primes describe the derivatives with respect to the spacelike worldsheet coordinate, which is normally represented by σ .

It is worth explaining the physical meaning of these conditions. The first one tells us that the velocity of the string will always point in the direction perpendicular to its local tangent vector, while the second one fixes σ to parametrize the energy along the domain wall string. The interesting thing about this gauge is that the equations of motion become

$$\ddot{\mathbf{X}} - \mathbf{X}'' = 0 , \quad (25)$$

which is simply the wave equation for the 2-vector, $\mathbf{X}(\sigma, t)$. The solution of these equations is well known and can be written in terms of right-movers and left-movers along the wall as

$$\mathbf{X}(t, \sigma) = \frac{1}{2} (\mathbf{a}(\sigma - t) + \mathbf{b}(\sigma + t)) , \quad (26)$$

where in order to fulfill the gauge conditions the functions \mathbf{a}' and \mathbf{b}' must satisfy

$$|\mathbf{a}'(\sigma)| = |\mathbf{b}'(\sigma)| = 1 . \quad (27)$$

In the following, we will use this type of solutions in several different ways. First, we will make use of this gauge to design simple initial conditions for the numerical experiments that we will perform in the following section to check the validity of the Nambu-Goto action. Moreover, we will also apply this parametrization of the string to identify the (Nambu-Goto) initial data at any point in the evolution of the string and predict the subsequent evolution according to this approximation. This will allow us to make a comparison of the string motion with the Nambu-Goto prediction at an arbitrary point during our simulations. We describe this technique in more detail in Appendix A 3.

A. Testing the validity of the Nambu-Goto action

The Nambu-Goto action is an approximate description of the full dynamics of field theory domain walls. There are different types of corrections that we can think of. First, there is

¹¹ For more details, see [21].

the possible effect of radiation that we have already discussed in the previous section. The results there indicate that one can neglect these effects for low curvature domain walls.

Furthermore, it is also clear that the Nambu-Goto action is only strictly applicable to an infinitely thin wall. Therefore, if we want to apply it for field theory objects, there are additional terms that need to be included in the effective action. In fact, one can think of the NG action as the first term of an effective action built as an expansion in powers of the ratio of the thickness of the string to its radius of curvature. This has been studied in some detail in several papers in connection to strings and domain walls [22–25]. Of course, there will also be instances where both these effects could be important.

In the following sections, we will numerically evolve several initial conditions and study the validity of the Nambu-Goto action and the circumstances where corrections play a significant role.

1. *Colliding wiggles on a straight domain wall*

Here we will closely follow the setup studied in the case of local cosmic strings in [12] and discuss the collision of wiggles on a straight domain wall. In order to accurately compare the evolution of the soliton with the NG prediction, we need to start with an initial condition that is close enough to an exact solution of the full field theory equations. Otherwise, the possible deviations from the NG dynamics could just be due to the lack of precision in the initial configuration.

In this case, it is actually possible, using the results presented in [19], to set an initial condition that is extremely close to an exact solution of the non-linear scalar field theory. Let us describe how to construct this solution in detail.

Let's suppose once more that the domain wall is extended along the y direction, and consider a field configuration of the form

$$\phi(x, y, t) = \phi_K [x - \psi_+(y + t) - \psi_-(y - t)], \quad (28)$$

where $\phi_K(x)$ is the domain wall profile and $\psi_+(y + t)$ and $\psi_-(y - t)$ represent wiggles propagating in opposite directions on the wall. Using the results of [19], it is clear that this is in fact a configuration that can be made to be arbitrarily close to an exact solution initially provided that the two functions $\psi_+(y + t)$ and $\psi_-(y - t)$ do not have significant overlap. For small amplitudes, these propagating wiggles correspond to the linear zero mode excitations of the type presented in (9).

So, what should we expect from these collisions? Let us first consider the situation where the functions describing these wiggles are very mildly curved, so even if we overlap them there would never be a point of large curvature for the domain wall. In this case, we will

expect the NG prediction to be accurate. Furthermore, looking at the expression in Eq. (26) it is clear how to construct the NG initial data for this configurations. Once we have the information for the functions $\mathbf{a}(\sigma)$ and $\mathbf{b}(\sigma)$ we can easily obtain the NG result for later times. This is all we need to compare the field theory result, the one we obtain evolving the complete field theory equations in a $(2 + 1)d$ lattice, and the NG predictions.

At small amplitudes for the displacement of the wiggles, one would expect them to propagate at the speed of light almost unaffected by the presence of the other one. This behaviour at small amplitudes can be explained by the fact, discussed earlier, that wiggles on the string are perturbatively described by zero modes at a linearized level.

However, the NG action is non-linear, as we stressed earlier. Therefore, we would like to explore the situations where we can probe these non-linearities. In other words, the NG action is a resummation of an effective action for all orders in first derivatives of the displacements from the straight domain wall, so in order to check this special structure of the theory one should go beyond linear order.

On the other hand, the generic solution in the conformal gauge given by Eq. (26) seems to indicate that arbitrary wiggles colliding on a straight domain wall would just pass through one another unaffected in their shape, so it is not clear what the non-linearities do even in the large amplitude case.

The resolution of this puzzle is best explained in the static gauge. In this case, one chooses the worldsheet coordinates to be aligned with the straight wall, namely, we take

$$X^0 = t, \quad X^1 = y . \quad (29)$$

The NG action in this case can be written as

$$S_{SG} = -\mu \int dt dy \sqrt{1 + \psi'^2 - \dot{\psi}^2} . \quad (30)$$

In this form, this is the action for a scalar field $\psi(y, t)$ living on a $2d$ worldsheet with a Born-Infeld type Lagrangian. The equation of motion from this action becomes

$$\partial_t \left(\frac{\dot{\psi}}{\sqrt{1 + \psi'^2 - \dot{\psi}^2}} \right) - \partial_y \left(\frac{\psi'}{\sqrt{1 + \psi'^2 - \dot{\psi}^2}} \right) = 0 . \quad (31)$$

It is clear that a particular set of solutions of these equations is given by waves moving at the speed of light along a straight domain wall. In other words, functions of the form $\psi(y \pm t)$ would be solutions of this equation. In this way we recover the Vachaspati-Vachaspati configurations [19] within the Nambu-Goto description. However, the equation is clearly non-linear and only when we have small amplitudes we will approximately recover the linear wave equation for a generic configuration $\psi(y, t)$.

It is easy to see that the effect of the non-linear terms is only to create a delay in the wiggles as they pass through one another. This delay can be computed and it turns out to be proportional to the extra energy on the string due to the existence of each of these wiggles. This is not surprising since the difference between the parameter σ in the NG solutions in the conformal gauge and the space coordinate y which parametrizes our solutions in this other gauge is indeed given by this amount of energy¹².

Thinking in terms of the conformal gauge solution helps us understand this scattering process. Since the theory is integrable, the wiggles can not change their shape or produce $(1+1)d$ radiation in the collision. Therefore, it is obvious that this is the only possible outcome of this interaction between the asymptotic waves. This type of behaviour is reminiscent of the interaction of solitons in integrable models like the Sine-Gordon equation [18].

We have checked these predictions of the NG approximation by performing several different numerical simulations in field theory and comparing them with the results expected from the NG dynamics. In order to do this, we have developed a method of reconstruction of the NG evolution from the position and velocity of the domain wall string in field theory. See the Appendix A 3 for the details of this reconstruction method.

We started by considering the collision of two wiggles designed in such a way that their NG evolution would lead to a domain wall configuration with a small curvature everywhere. Our simulations show that the NG prediction in this case is indeed perfect. The reconstructed NG energy stays constant and the position of the string obtained directly from the simulation agrees precisely with the one predicted in NG (see Fig. 5).

Furthermore, we also plot the position that the wiggles would have if the solution was just the wave equation. We can see in Fig. 5 a comparison between these different situations, where we can easily appreciate the delay in the field theory simulation due to the non-linear NG interactions. This is also in perfect quantitative agreement with the NG description. We also plot in this figure the predicted position of the peak of the wiggles assuming the delay is given by the extra energy of the oppositely moving wiggle with respect to the straight string. We note the agreement is again perfect. We have also performed this type of experiments with asymmetric wiggles and found, in all cases, a perfect agreement between the numerical

¹² To be more precise, we can think about a small wiggle first propagating on a long straight string. In this case there is no distinction between the coordinate y and the amount of energy that the wiggle traverses, σ . However, as the wiggle encounters the oppositely moving large excitation, these two quantities are not the same. The NG dynamics tells us that this small wiggle will travel at the speed of light in (t, σ) space and not in (t, y) space. The difference between these two quantities is exactly the extra energy of the wiggle with respect to the straight string. Hence, there will be a delay in the position of the little wiggle after the collision between its actual position and the value of the y coordinate one would (erroneously) predict assuming that it had propagated at the speed of light in the (t, y) coordinates.

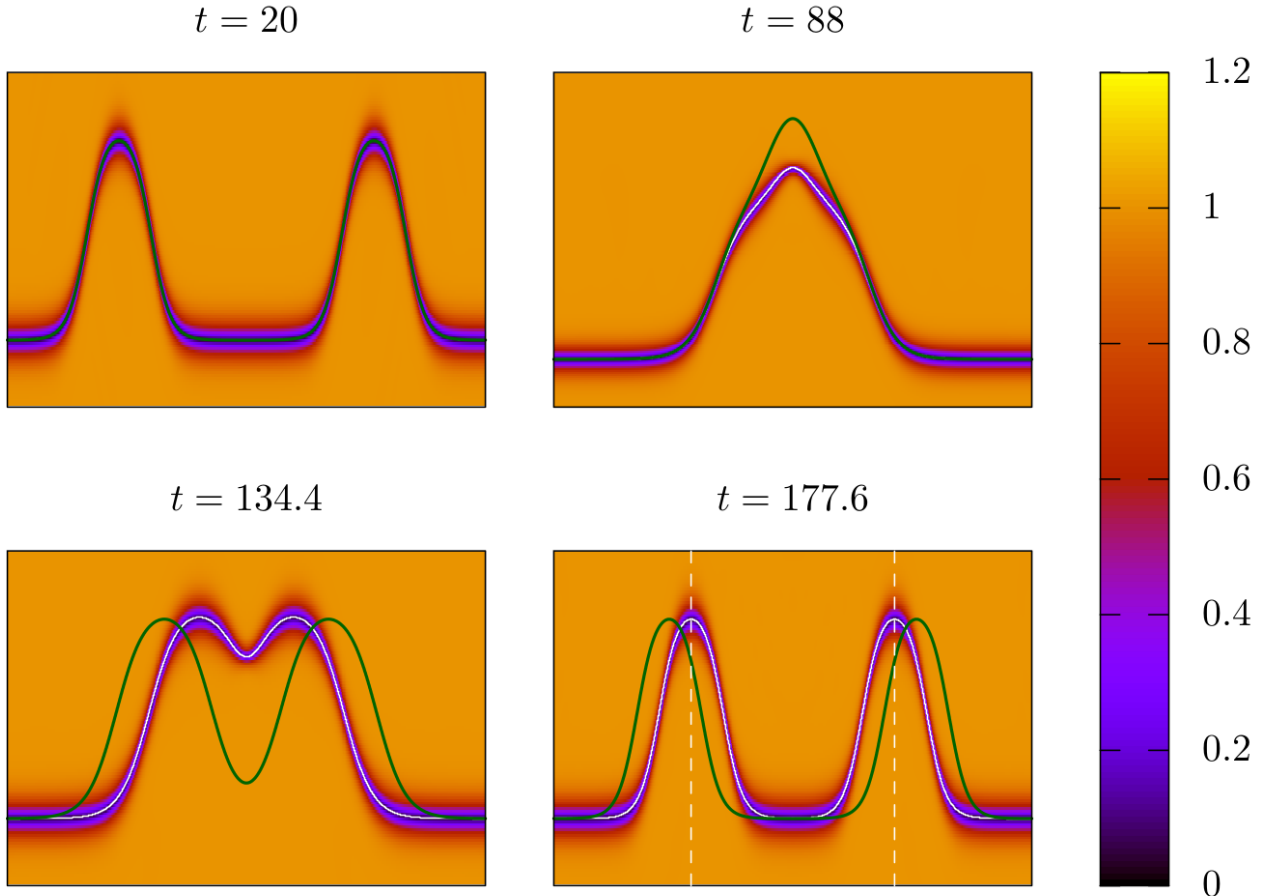


FIG. 5: Field theory simulation of the collision of low curvature wiggles propagating on a straight domain wall string. We show the absolute value of the field, ϕ/η , in the 2-dimensional simulation space (note that according to our prescription in the main text the straight domain wall string is extended along the y direction, which here corresponds to the horizontal axis). The white curve represents the position of the domain wall string according to the NG approximation, while the green curve corresponds to the solution of the linear wave equation. Finally, the dashed vertical lines represent the predicted position of the peak of the wiggles taking into account their time delay due to the non-linearities of the NG equation of motion. The time labels are displayed in units of $(\sqrt{\lambda}\eta)^{-1}$, and the ranges of x and y in these units are the following: $y \in [-150, 150]$ and $x \in [-5, 20]$ for the $t = 20$ and $t = 177.6$ panels, $y \in [-100, 100]$ and $x \in [-5, 30]$ for the $t = 88$ panel, and $y \in [-100, 100]$ and $x \in [-5, 20]$ for the $t = 134.4$ panel.

results and the analytic NG description.

Finally, we visualize this delay by plotting in Fig. 6 the position of the center of the wiggles in a (y, t) spacetime diagram.

We have also let the wiggles interact several times by imposing periodic boundary con-

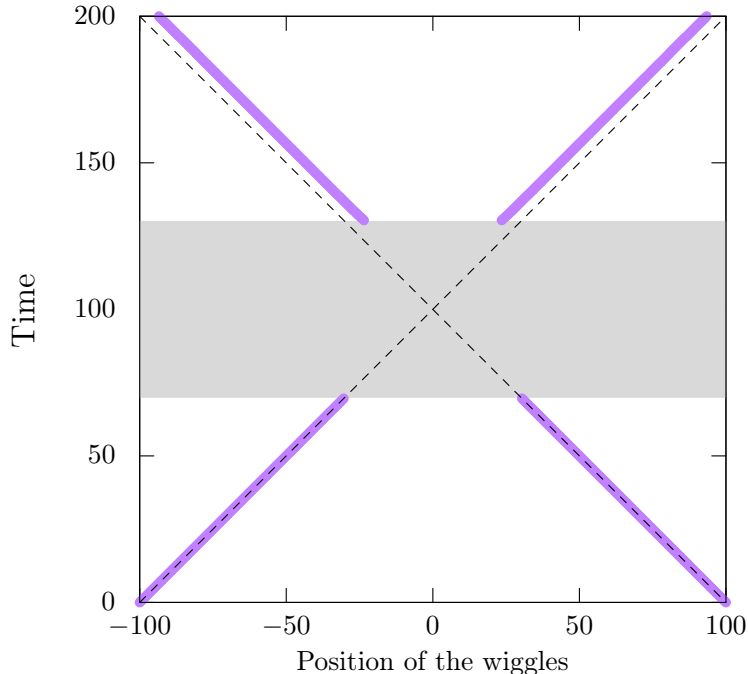


FIG. 6: Spacetime diagram for the position of the wiggles propagating on the straight domain wall string obtained directly from the field theory simulation (in purple) and for speed of light propagation (dashed line). The shaded grey region indicates the time during which the wiggles overlap.

ditions on the y axis. The results continue to be in perfect agreement with NG even for a large number of collisions.

Finally, we have also explored the scattering of wiggles that lead to the formation of high curvature regions. We show in Fig. 7 the amount of energy in the box in our numerical simulations. We see the different steps where the energy is depleted by the bursts of radiation from the high curvature regions. This is very similar behaviour to the one presented in [12]. After the collision, the domain wall behaves again like a NG soliton with wiggles of different shape.

In summary, we have checked explicitly that the non-linear behaviour of the NG action reproduces perfectly the solution seen solving the full field theory equations in the case of small curvatures for the domain wall.

2. Standing waves

In this section, we compare the evolution of a zero mode excitation in the form of a standing wave in the NG description with the actual solution from field theory. Similarly

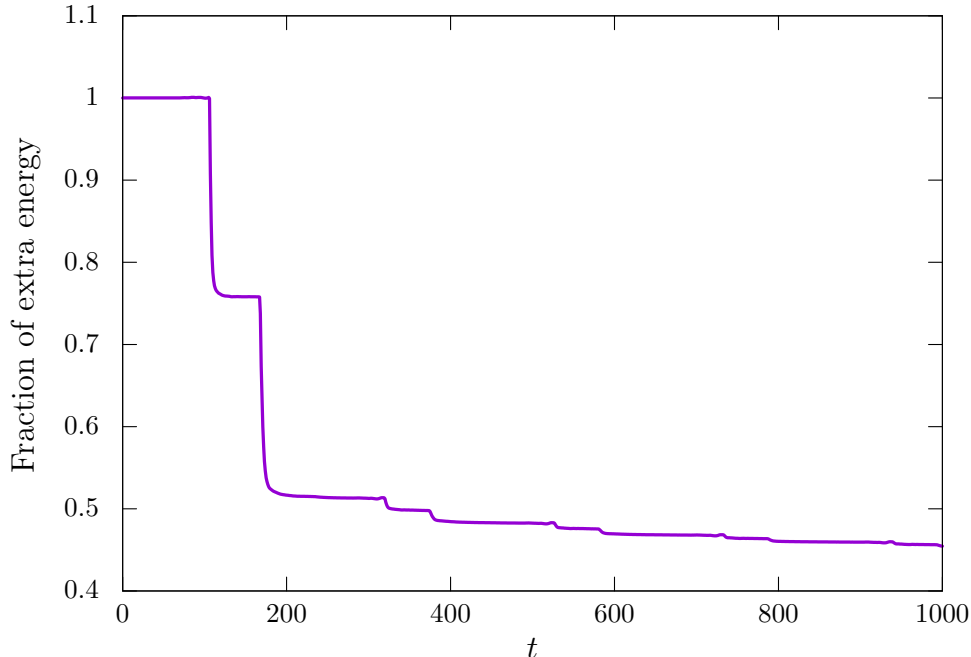


FIG. 7: Fraction of extra energy as a function of time, displayed in units of $(\sqrt{\lambda\eta})^{-1}$, for high curvature wiggles colliding on the wall. “Extra energy” means total energy inside the box minus energy of the straight domain wall, or in other words, the energy on the wiggles on the straight domain wall. In this case, the maximum ratio of string thickness to radius of curvature is approximately $\kappa \approx 0.44$ at the moment of the collision.

to what we use in section IIIA, we will take our initial conditions for the standing wave in field theory to be the ones described by Eq. (13). We stress that these are not exact initial conditions, but only approximate ones. However, following the arguments in Appendix B, we will consider them a good enough approximation for our purposes. Furthermore, choosing the amplitude and the frequency of the standing wave with some care (see Eq. (16)), we can study the behaviour of solutions within the small curvature regime where the NG action should be valid.

We analyze different values of the frequency of oscillation, some below the threshold of the massive particles in the bulk and some above. The results show that for frequencies below the threshold the amount of radiation is negligible and the position of the wall stays within the NG solution for extremely long periods of time. We compare both the position of the domain wall with the NG prediction as well as the energy from the NG reconstruction. Both measures indicate a very good agreement with the NG description. For higher frequencies, the emission of radiation reduces the NG energy in time in agreement with the prediction from the analytic estimates of Appendix C 1.

For larger amplitudes but frequencies below the threshold of radiation, the agreement

with NG becomes less precise. The reconstructed NG energy is still more or less constant, but the position of the domain wall is slightly different from the NG dynamics. This may be an indication of the effect of higher order terms in the effective action missing in the NG dynamics. However, this is hard to quantify since increasing the amplitude some more one starts seeing the effects of non-perturbative radiation so it is difficult to disentangle both effects.

Our results in this section confirm the expectation that the NG action describes very accurately the evolution of domain wall strings without any internal excitation. This agreement ceases to be perfect only in the presence of high frequency oscillating modes where some radiation is possible. This was also expected since at those frequencies one can start exciting the massive degrees of freedom that could propagate in the bulk carrying away part of the energy of the domain wall string. Finally, regions of high curvature also lead to deviations from NG and the emission of energy by a non-perturbative process; a sort of high curvature annihilation.

V. EFFECTIVE THEORY INCLUDING THE INTERNAL MODE

As we described earlier, the presence of excitations localized on the domain wall could add a substantial amount of energy to the configuration. This suggests that one could change the dynamical properties of the soliton by this excitation process. This is somewhat similar to what happens with superconducting cosmic strings, where the current on the string core effectively modifies the equation of state of the string [26, 27].

A simple strategy to quantify this effect would be to analyse the energy momentum tensor for the excited domain wall as a function of the amplitude of the internal mode. This will give us an idea of the kind of change we could expect in its dynamics for a given amount of extra energy in the excitation.

In order to do that, we consider the simple field configuration of a homogeneously excited straight wall of the form

$$\phi(x, y, t) = \phi_K(x) + A(t) \times f_1(x) , \quad (32)$$

and insert it in the expression for the energy momentum tensor of the scalar field. After integrating over the transverse x direction, one obtains, at a quadratic order in the amplitude of the excitation, the following expression for the energy per unit length and tension of the domain wall string,

$$\mu_A = \mu \left(1 + \frac{9}{8\sqrt{2}} \frac{\sqrt{\lambda}}{\eta} \hat{A}^2 + \dots \right) \quad (33)$$

and

$$\tau_A(t) = -\mu \left(1 + \frac{9}{8\sqrt{2}} \frac{\sqrt{\lambda}}{\eta} \hat{A}^2 \cos(2\omega_s t) + \dots \right), \quad (34)$$

where we have assumed that the evolution of the shape mode is well approximated at quadratic order by a periodic function of the form¹³ $A(t) = \hat{A} \cos(\omega_s t)$.

One can obtain this type of energy momentum tensor postulating the existence of a domain wall with an extra scalar degree of freedom living on its worldsheet. The simplest effective action of this kind is given by

$$S = \int d^2\xi \sqrt{-\gamma} \left[-\mu + \frac{1}{2} \gamma^{\alpha\beta} \partial_\alpha \theta \partial_\beta \theta - \frac{1}{2} m_\theta^2 \theta^2 \right], \quad (35)$$

where as before γ parametrizes the induced metric on the worldsheet and the scalar field $\theta(\xi^a)$ characterizes the amplitude of the internal mode excitation provided that we choose $m_\theta = \frac{\sqrt{3}}{2} m$.

At a linear order, this theory describes the free degrees of freedom propagating on the straight domain wall, namely, the massless Goldstone modes and the massive internal mode. These are just the fluctuation modes we identified in the previous section. Taking it beyond the linear order, the theory describes a non-trivial interaction between these modes which could lead to interesting effects.

On the other hand, it is clear that the massive mode in this 1 + 1 dimensional theory introduces a new time scale associated with its oscillating period $\tau_m \sim 1/m_\theta$. For times much larger than this, the average effect of the excitation on a straight domain wall is to increase its energy density but does not modify its tension. For a uniformly excited wall, this would seem to decrease the speed of propagation of the transverse excitations of the string. Thinking about a closed loop, this would also seem to slow down the collapse of the loop.

However, it is important to remember that this effective action disregards any radiative effect. This means that in order to use it we should only consider situations where the excitations are not large enough to create a substantial amount of radiation in the period of time that we are interested in. Otherwise, the real dynamics of the domain wall in field theory would be very different from the one inferred from this action.

As we described in detail in previous sections, the presence of an excited domain wall leads to radiation on a time scale that is inversely proportional to the square of the amplitude of the excitation. This means that if we are interested in studying the implications of this effective action over long periods of time we should only consider the case with small

¹³ This assumption receives corrections when one includes higher order terms, but we will limit ourselves with these leading order terms for now.

amplitude values for θ . However, in this case, the possible deviations from the Nambu-Goto action would therefore be small. One could try to incorporate these effects into this effective action, but it is not clear to us how to do this in an accurate way.

Alternatively, one could always study the effects of these excitations by using field theory simulations in the lattice. We have done one such simulation of a collapsing domain wall ring initially at rest and excited in a uniform way. The results are presented in Appendix G, where we show how the evolution of the domain wall loop is slowed down by the presence of the extra energy associated to the scalar field perturbation. This is in agreement with the results obtained from the effective action given by Eq. (35). However, a detailed comparison of this type of configuration with the results obtained from this effective action is difficult due to the presence of extra radiation for large values of the amplitude of the excited state.

A. Parametric resonance within the effective action description

Let us conclude this section by indicating another important effect that is already hinted in our effective action approach. As one can see in Eq. (34), the value of the tension of the domain wall oscillates in the presence of internal modes. This suggests that one could have parametric resonance effects that would stimulate the appearance of transverse excitations on the position of the wall. This is the analogue effect to the non-relativistic string resonance already discussed a long time ago in [28]. Indeed, one can easily show this behaviour by looking at the equation of motion for the position of the domain wall string from our effective action, namely the equation

$$\partial_a [\sqrt{-\gamma}(\mu\gamma^{ab} + T^{ab})\partial_b X^\mu] = 0, \quad (36)$$

where T^{ab} denotes the $(1+1)d$ energy momentum tensor associated with the scalar field describing the bound state amplitude, the scalar field θ . Assuming the lowest order solution for the scalar field equation of motion, we take $\theta(t) = \theta_0 \cos(w_s t)$.

Let us now consider a string extended along the y direction that is parametrized in the form $X^\mu(t, y) = (t, \psi(t, y), y)$. And for simplicity let us take the displacement of the string to be $\psi(t, y) = D(t) \cos(w_0 y)$. Within this ansatz, the equation for the amplitude of the string displacement is given by

$$\ddot{D}(t) + w_0^2 \left(1 - \frac{\dot{\theta}^2}{\mu}\right) D(t) = 0, \quad (37)$$

which for our oscillating scalar field transforms into a form of the Mathieu equation. This shows that this type of internal mode excitation can create a parametric instability in the position of the domain wall of a form of a standing wave of frequency equal to the bound state frequency, namely, $w_0 = w_s$.

In the following section we will explore the presence of these instabilities in full detail at the non-linear level with the help of our numerical simulations. In fact, we will see that these are not the only source of parametric resonance effects present in field theory.

VI. PARAMETRIC RESONANCES FROM FIELD THEORY SIMULATIONS

A. Dimensionless variables

From now on, to make the comparison to our numerical simulations more direct, we will work with the following set of dimensionless variables:

$$\tilde{\phi} = \phi/\eta, \quad \tilde{t} = \sqrt{\lambda}\eta t, \quad \tilde{x} = \sqrt{\lambda}\eta x, \quad \tilde{y} = \sqrt{\lambda}\eta y. \quad (38)$$

With this rescaling, the action reads

$$S = \frac{\eta}{\sqrt{\lambda}} \int d^3\tilde{x} \left[\frac{1}{2} \partial_\mu \tilde{\phi} \partial^\mu \tilde{\phi} - \frac{1}{4} (\tilde{\phi}^2 - 1)^2 \right], \quad (39)$$

where the partial derivatives are now with respect to the dimensionless spacetime coordinates. The mass of small fluctuations about the vacuum, the energy per unit length of the static domain wall solution and the angular frequency of the homogeneous shape mode are now given by $\tilde{m} = \frac{m}{\sqrt{\lambda}\eta} = \sqrt{2}$, $\tilde{\mu} = \frac{\mu}{\sqrt{\lambda}\eta^3} = \sqrt{8/9}$ and $\tilde{\omega}_s = \frac{\omega_s}{\sqrt{\lambda}\eta} = \sqrt{3/2}$, respectively. Moreover, the amplitude of the shape mode will be rescaled as $\tilde{A} = \lambda^{1/4} \hat{A} / \sqrt{\eta}$, which is still dimensionless.

In the following we will drop the tildes for simplicity, but all variables will refer to these new dimensionless quantities.

B. A parametric instability for a homogeneous internal excitation

As we pointed out in the previous section, the perturbation of a domain wall by an internal mode can lead to the subsequent excitation of a particular zero mode. This type of parametrically resonant excitations of the transverse position of the string by perturbations on its tension have been known and studied for a long time. In fact, this is one of the first examples of parametric resonance events in the history of physics [28].

The simplest way to see this phenomenon in our field theory context is to assume a particular ansatz for the perturbations around the static straight domain wall of the form

$$\phi(t, x, y) = \phi_K(x) + A(t)f_1(x) + D(t)f_0(x) \cos(\omega_0 y) , \quad (40)$$

where $f_0(x)$ and $f_1(x)$ are given by the wave functions found in Section II B. We will consider the string to be in a box with periodic boundary conditions along the y direction. This is, of course, a particular truncation of the most generic type of ansatz we can write. In particular, we are disregarding any coupling of this configuration to any radiating mode. This would only be consistent with our findings in the previous sections if we assume that the amplitudes of the modes involved in this calculation are sufficiently small.

Plugging this expression in the equation of motion for the scalar field and projecting the result onto the different mode functions of the perturbations, we arrive to a set of coupled differential equations for the amplitudes of the different modes¹⁴:

$$\ddot{A}(t) + \frac{3}{2} [1 + C_1 D^2(t)] A(t) + 6C_2 A^2(t) + \frac{3C_1}{2} A^3(t) + \frac{3C_2}{2} D^2(t) = 0 , \quad (41)$$

$$\ddot{D}(t) + [\omega_0^2 + 6C_2 A(t) + 3C_1 A^2(t)] D(t) + \frac{9C_1}{4} D^3(t) = 0 , \quad (42)$$

where the numerical coefficients come from the projection over the x direction and are given by $C_1 = 3\sqrt{2}/35$ and $C_2 = 3\sqrt{3}\pi/(64 \cdot 2^{3/4})$.

Taking the limit of $D = 0$ of this system of equations we obtain the non-linear equation for the oscillation of the internal mode. Reducing the equation to the linear order we recover the result that the internal mode oscillates with a frequency $\omega_s = \sqrt{3/2}$.

Let us now consider the equation for the amplitude of the zero mode. Taking the lowest order approximation of this equation we arrive at

$$\ddot{D}(t) + [\omega_0^2 + 6C_2 A(t)] D(t) = 0 . \quad (43)$$

Assuming that the shape mode is excited at a linear order, we can substitute its amplitude in this equation with the expression $A(t) = \hat{A} \cos(\omega_s t)$. Doing this substitution, we can identify that the resulting equation is nothing but a particular form of the Mathieu equation [29]. This type of equation has been extensively studied in the context of parametric resonance in different physical phenomena. The results of these studies indicate that the solution of this equation has several bands of instability centered around particular values of the frequency ω_0 where its amplitude would grow exponentially with time¹⁵. In our case, this translates to a region of instability around $\omega_0 \approx \omega_s/2$.

¹⁴ See the Appendix D for a detailed explanation of this procedure.

¹⁵ See the brief discussion in the Appendix E of the most relevant aspects of the Mathieu equation and its connection with our problem here.

Note that this is a different resonant frequency than the one obtained from the effective action in the previous section. The reason for this is clear: the resonant effect comes in this field theory language from a linear term in the amplitude of the internal mode, while it is of quadratic order in the effective action description. We will comment more on this in the next section, but let us just mention that a quadratic driving resonant term also appears in the field theory equations in Eq. (42). However, as the amplitude of the internal mode is small, this term will not be the dominant one here. In order to test this prediction, we perform a field theory simulation in a lattice.

Following the previous calculation we will expect that the homogeneous initial configuration of a domain wall with an excited internal state would resonantly produce a transverse perturbation of the form of standing waves with frequency $\omega_0 \approx \omega_s/2$. We show in Fig. 8 several snapshots of the position of the domain wall for this type of configuration from our numerical full field theory simulations. For this example, we took the initial conditions to be

$$\phi(x, y, t = 0) = \phi_K(x) + A(0)f_1(x) + D(0)f_0(x) \cos(\omega_0 y) , \quad (44)$$

$$\dot{\phi}(x, y, t = 0) = 0 , \quad (45)$$

with $\omega_0 = 2\pi/10$, $A(0) = 0.5$ and $D(0) = 0.02$. It is clear from the images that a transverse modulation of the wall grows over time, becoming really noticeable in agreement with the previous analytic considerations.

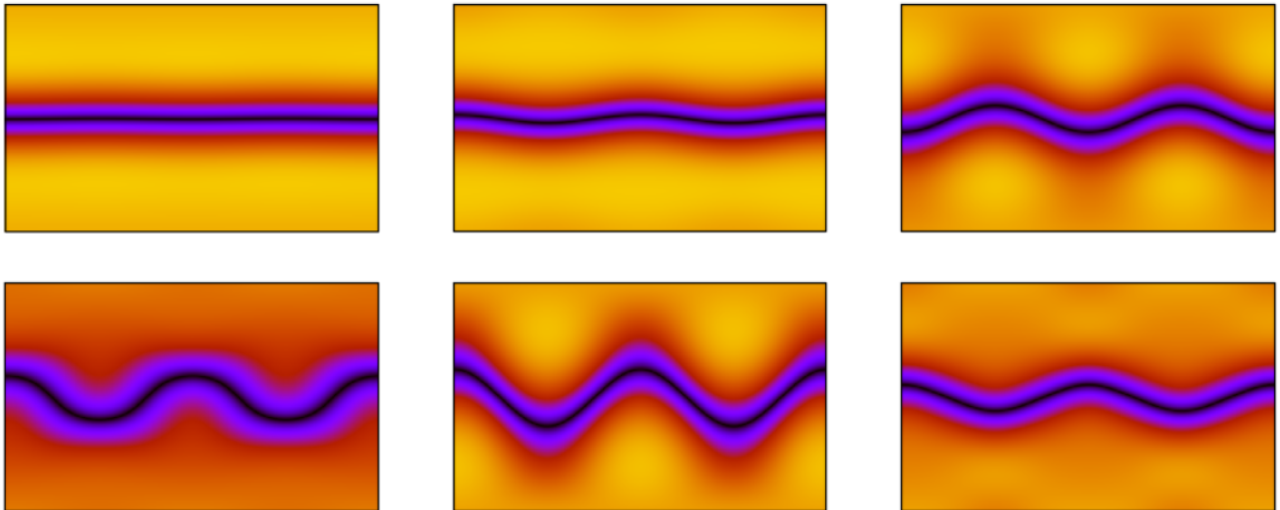


FIG. 8: Parametric resonance excitation of a standing wave for the position of the domain wall string with frequency $\omega_0 \approx \omega_s/2$ for a homogeneous initial state with an internal mode excitation of frequency ω_s . In these plots, x ranges from -4 to 4 (vertical axis), and y from -10 to 10 (horizontal axis).

This exponential growth is eventually tamed by the higher order terms in the different amplitudes of the modes that we have neglected in our discussion. In particular, as the zero mode amplitude grows, the one for the shape mode decreases. This is basically a process of energy transfer between these modes. After a while, the non-linear source term proportional to $D^2(t)$ in the equation for the amplitude of the shape mode becomes important. This term drives the amplitude for the shape mode back up to its original value, depleting, in turn, the amplitude of the zero mode. This completes the full cycle and brings the system to the initial state.

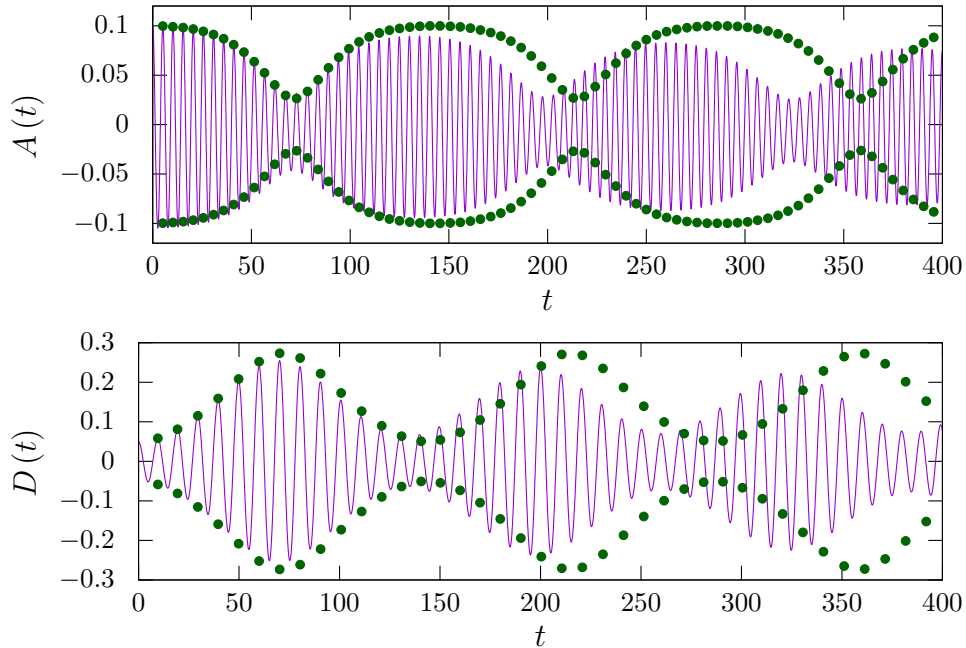


FIG. 9: Amplitude of the shape mode (top panel) and the resonant zero mode (bottom panel) as a function of time. The values read from the simulation are shown in purple, and the green dots correspond to the solution of the coupled equations (41) and (42). In the latter case, we only show the envelope in order to make the comparison easier.

We have performed several numerical simulations for an initial homogeneous state of an excited domain wall. Using the orthogonality condition of the modes that describe the linear perturbations of the static domain wall solution, we can extract directly from the simulation the values of the amplitudes of these modes as a function of time. We have done this for a particular run and compared the results with the numerical solution of the reduced set of Eqs (41) and (42). The results are shown in Fig. 9. Although the first pulse is predicted almost perfectly by the coupled equations, the subsequent ones deviate appreciably presumably due to the presence of radiation being emitted in the process. Indeed, we do observe this radiation in our simulations.

C. A standing wave on the internal mode

Following the discussion in the previous section, we would like to explore now the possibility of other resonant phenomena in more generic situations. In particular, we will consider the case where the internal mode has the form of a standing wave. In this case, we can show that the initially straight domain wall develops an instability towards the formation of a standing wave with a couple of different wavelengths (see the snapshots in Fig. 10).

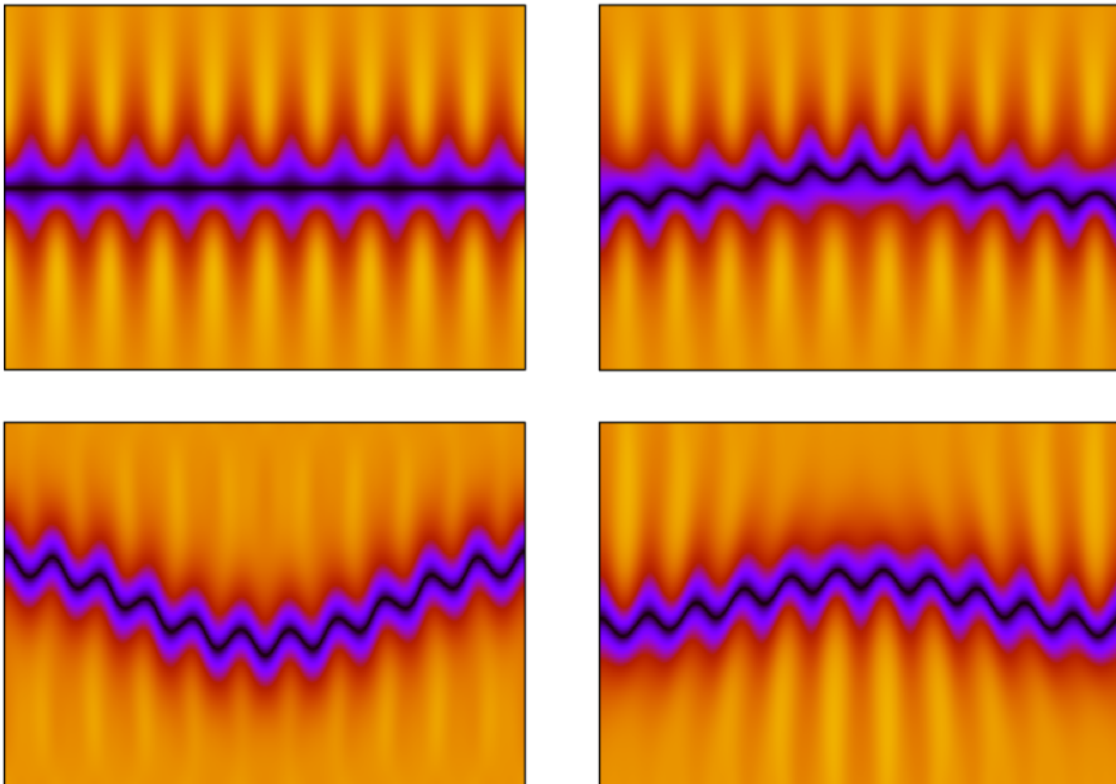


FIG. 10: Standing wave in the internal mode decaying into a standing wave on the position of the domain wall string with two different frequencies. In these plots, x ranges from -5 to 5 (vertical axis), and y from -17 to 17 (horizontal axis).

We can explain this behaviour by taking the ansatz

$$\phi(t, x, y) = \phi_K(x) + A(t)f_1(x) \cos(k_s y) + D_1(t)f_0(x) \cos(k_1 y) + D_2(t)f_0(x) \cos(k_2 y) . \quad (46)$$

The resultant equations of motion at the lowest order for the time dependent amplitudes of the different modes turn out to be, after the projection on the x and y directions,

$$\ddot{A}(t) + \left(\frac{3}{2} + k_s^2 \right) A(t) + 3C_2 D_1(t) D_2(t) = 0 , \quad (47)$$

$$\ddot{D}_1(t) + k_1^2 D_1(t) + 3C_2 A(t) D_2(t) = 0 , \quad (48)$$

$$\ddot{D}_2(t) + k_2^2 D_2(t) + 3C_2 A(t) D_1(t) = 0 , \quad (49)$$

where $C_3 = 9\sqrt{3}\pi/(64 \cdot 2^{3/4})$. These are the correct equations for the amplitudes as long as the following three conditions are met: (1) $k_1 \neq k_s/2$, (2) $k_2 \neq k_s/2$ and (3) $k_1 + k_2 = k_s$ or $|k_1 - k_2| = k_s$. This kind of system of coupled equations has been discussed before in the literature in connection with mechanical systems (see for example [30]). The results in these papers indicate that one can find solutions where a simultaneous resonant amplification of two different modes is possible provided that their wavenumbers satisfy the condition

$$k_1 + k_2 = \Omega_s = \sqrt{\frac{3}{2} + k_s^2}. \quad (50)$$

One can in fact find bands of instability quite similar in nature to the ones in the Mathieu equations, so this condition does not have to be completely sharp. If we also take into account condition (3) above, we should expect amplification of two zero modes with frequencies $k_1 = (k_s + \Omega_s)/2$ and $k_2 = (-k_s + \Omega_s)/2$. This is exactly what we have found in our numerical simulations of the excited domain wall in a box¹⁶. For the simulation shown in Fig. 10, we took the following initial conditions:

$$\phi(x, y, t = 0) = \phi_K(x) + A(0)f_1(x) \cos(k_s y), \quad (51)$$

$$\dot{\phi}(x, y, t = 0) = 0, \quad (52)$$

with $k_s = 10\pi/17$, $A(0) = 0.4$.

D. An effective action including higher order interactions

As we mentioned already, the parametric resonance predicted using the effective action in Eq. (35) yields a different result for the resonant zero mode frequency of excitation than the one found in field theory. This discrepancy can be traced to the relevant oscillatory term in the associated Mathieu equations. In the effective theory description, that term is quadratic on the amplitude of the internal mode. However, in the field theory account of this effect, the relevant term is linear. This explains the doubling of the resonant frequency between both models.

An interesting question that we might ask is whether we can supplement the effective action given by Eq. (35) in such a way that it can accommodate the coupling between the modes that we have uncovered in the previous section in the field theory simulations.

¹⁶ There is an added difficulty in our setup due to the periodic boundary conditions along the y direction. This adds the extra condition to the appearance of the instability due to the quantization of the wavenumbers along that direction.

One possibility could be the presence of terms of the form

$$S_{\text{curvature}} = \beta \int d^2\xi \sqrt{-\gamma} \theta(\xi) \mathcal{R}, \quad (53)$$

where the scalar field controlling the internal mode amplitude is coupled to the spacetime curvature of the domain wall string worldsheet (\mathcal{R}). Note that \mathcal{R} depends on derivatives of the position of the domain wall string X^μ . Therefore, this term describes a coupling between the internal mode and the Goldstone modes on the string. Terms of this form, without the coupling to the worldsheet scalar, have been proposed already in the context of higher order corrections to NG [22–25]. The interesting point about this addition to the effective action is that looking at the linearized equations of motion one identifies the appearance of a parametric resonance with the correct frequency (we show this in Appendix F). Furthermore, comparing the result with the field theory description, one can infer the value of the coefficient β in front of this term. Of course, this is not a proof that this is the correct term to the effective action, just that we can accommodate this particular coupling between the Goldstone mode and the internal mode with this term¹⁷. We leave the question of the relevance of these terms to be studied in a future publication.

E. New time scale of radiation

The discussion in the previous sections shows that the presence of excitations of the internal mode triggers the subsequent resonant excitation of Goldstone modes. This non-linear process can potentially also lead to radiation from the domain walls. Here we show that this is indeed what happens. We show in Fig. 11 the energy per unit length of an initially excited state in $1 + 1$ dimensions and compare it with the same case within a $2d$ box. The configuration in $1 + 1$ dimensions is, of course, prevented from exciting any longitudinal mode by construction and decays exactly according to the rate given by Eq. (C23) in the Appendix C2. Allowing for the domain wall to resonantly oscillate along the y direction, as in the simulation in the $2d$ box, induces a higher rate of radiation.

This demonstrates that the non-linear interaction between the internal mode and the Goldstone modes leads to a quicker emission of the extra energy in the form of the internal excitation. In other words, this interaction reduces the lifetime of the internal excitations.

¹⁷ It is reasonable to assume that there should also be a term similar to this one without the θ dependence in the effective action. However, this is not very relevant for our discussion here.

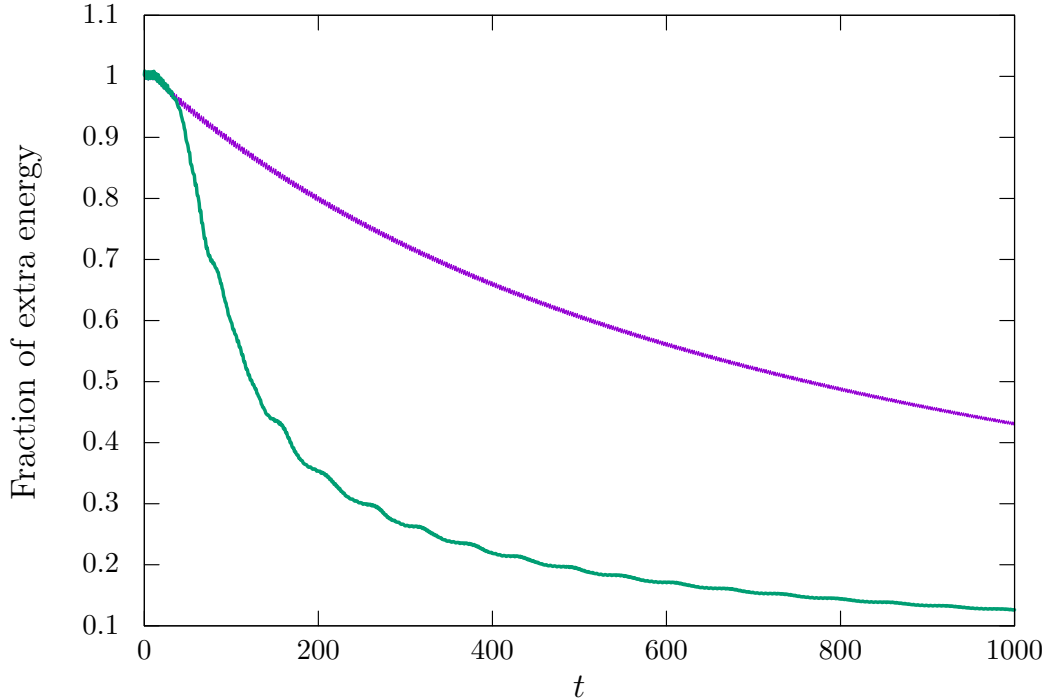


FIG. 11: Fraction of extra energy inside the box as a function of time in a $1 + 1$ simulation (purple curve) and in a $2 + 1$ simulation where the resonance occurs (green curve). “Extra energy” means additional energy with respect to the straight domain wall solution. The initial amplitude of the shape mode is, in this case, 0.3.

VII. DYNAMICAL EXCITATION OF THE INTERNAL MODES

One of the interesting points about the existence of internal excitations in these models is their relatively long lifetime. We have shown that for small amplitudes these excitations could survive for a time much larger than their natural time scale given by the thickness of the soliton. This makes these modes potentially relevant for numerical simulations where the time scale of the runs is shorter than the lifetime of these excitations.

Let’s now discuss what would be the evolution of these modes in a cosmological setting. In [4] we showed numerically that cosmological phase transitions would naturally lead to the formation of excited solitons. The typical amount of extra energy was found to be in the vicinity of 20% of the relaxed soliton mass¹⁸. It is therefore clear that one would have a period of time where the dynamics of the solitons could be affected by this extra energy by processes similar to the ones we discussed in previous sections. However, this period of time

¹⁸ Even though the simulations were performed in a simple $1 + 1$ dimensional lattice, we expect a similar behaviour in a more realistic $3 + 1$ dimensional scenario to yield comparable results.

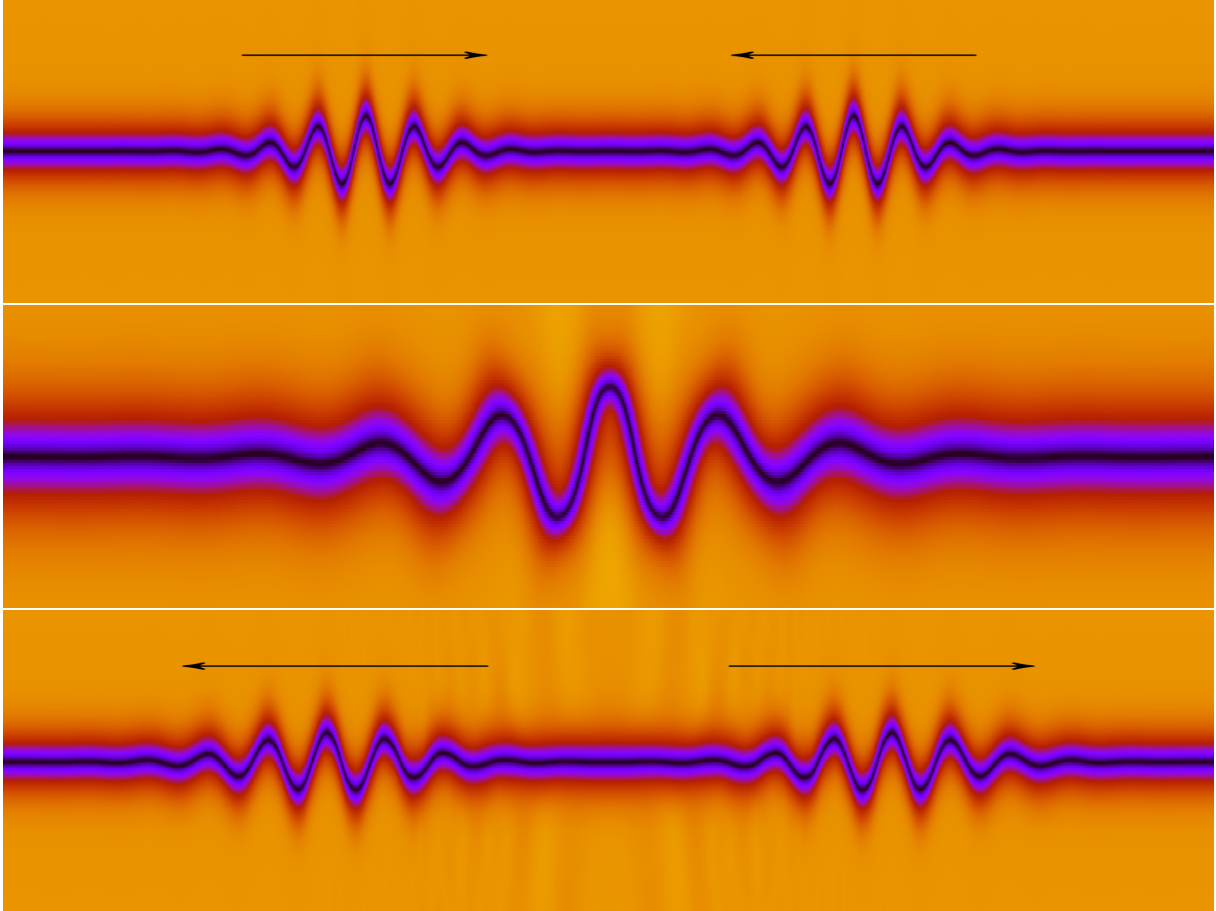


FIG. 12: Collision of two sinusoidal wave packets on the domain wall. We show the initial conditions at the top panel, the moment of maximum overlap in the middle and a configuration after the collision at the bottom. From top to bottom, the vertical axis x ranges from -8 to 8 , -4 to 4 and -8 to 8 , while the horizontal axis y ranges from -250 to 250 , -100 to 100 and -200 to 200 .

is still very small compared to the age of the universe, so we would like to ask whether there is any mechanism that would allow for the cosmological network of defects to replenish the level of excitation in the course of their evolution making these internal modes relevant for the long term dynamics of the real networks.

In order to study this possibility, we first imagine the case where the domain wall is relaxed and ask the question of whether the interaction between Goldstone modes could lead to a transfer of energy to the internal modes. This is a similar situation to the one we explored before in order to check the validity of the Nambu-Goto action, but now we are interested not only in the dynamics of the colliding wiggles but on the domain wall state that they leave behind. In particular, we will explore the collision between wiggles that are formed by a localized wavepacket with a single frequency mode in the region of their compact support. We take the initial conditions to be two of these packages separated by

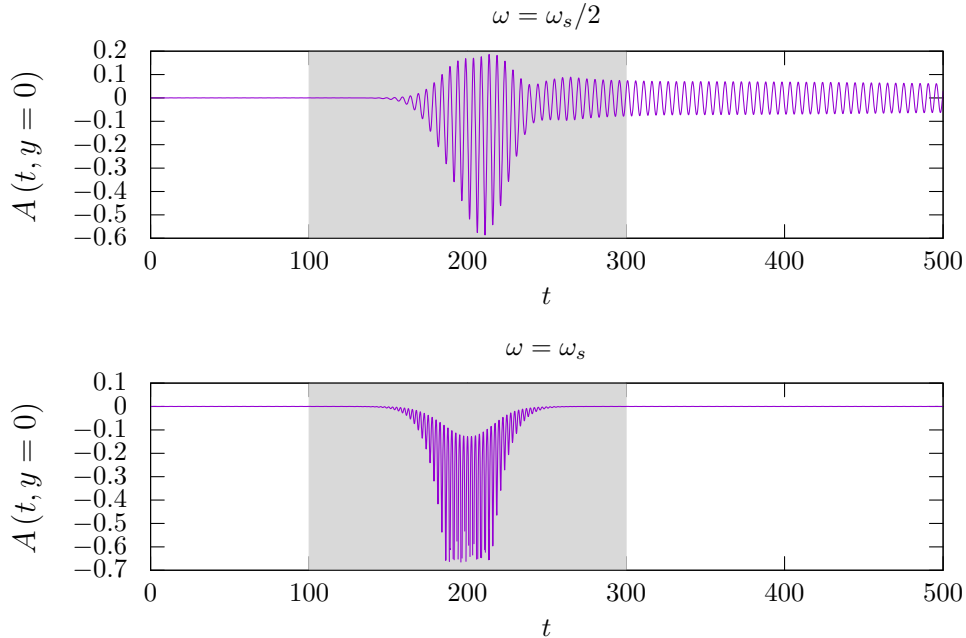


FIG. 13: Amplitude of the shape mode as a function of time at $y = 0$, the center of the box. The shaded region represents the time during which the wiggles overlap. The internal mode remains excited after the collision only when the frequency of the wiggles is $\omega = \omega_s/2$.

a distance in straight domain wall moving towards one another at the speed of light. After the collision, we study the straight segment of the domain wall left behind after the wiggles have passed through one another (see Fig. 12). One can analyze the amount of extra energy in this segment by projecting out the scalar field configuration onto the shape mode. Doing this, one can compute the amount of energy transferred from the wiggles to the internal modes as a function of the typical frequency of the wave packets¹⁹.

Our results indicate that the internal mode is not excited by any appreciable amount except in one particular situation. Taking the frequency of the wiggles to be half of the frequency of the internal mode, one can find an excited segment of the wall. This could be understood by looking at Eqs. (41) and (42). There we see that a zero mode fluctuation acts as a driving source for the internal mode. When the two wiggles overlap, one forms a standing wave for a short period of time with the appropriate frequency to resonantly excite the amplitude of the internal mode. Other frequencies do not create an amplification of

¹⁹ Note that the reconstruction of the excited mode during the time that the wiggles overlap (the shaded region in Fig. 13) is problematic due to the rapid motion of the domain wall. However, we are only interested in the result after the collision, where this projection can be trusted. We have checked that our results do not change by increasing the resolution in our lattice simulations.

these modes, as shown in Fig. 13.

This demonstrates that once the defects on the network have relaxed from their initial excited state it would be difficult to dynamically transfer energy to the internal modes since one would not expect a large amount of high frequency Goldstone modes on the walls at late times.

VIII. CONCLUSIONS AND IMPLICATIONS FOR COSMIC STRINGS

We have studied the dynamics of domain wall solitons that appear in a scalar field theory in $(2 + 1)d$. The lowest energy configurations of these solitons describe extended objects invariant along one of the spatial dimensions. They appear as line-like objects in our $(2 + 1)d$ setting, so we correspondingly name them domain wall strings.

We start our discussion by identifying the low energy excitations of these objects. These perturbations are divided in two different families of modes. The localized modes that represent small excitations around the background soliton solution and the radiative modes that describe vacuum excitations that propagate freely to infinity. Looking at the localized modes, we also distinguish two different types of perturbations. The Goldstone modes that parametrize the propagation of wiggles on the domain wall strings and the so-called shape mode that represents a change in the soliton's width.

We start by studying how the localized modes on the domain wall string lead to radiation. We obtain an analytic expression for the power emitted by the presence of wiggles on the string. In particular, we look at standing waves on the position of the string in the small amplitude regime. In this case we note that there is no radiation for wiggle excitations with frequency lower than $w_0 = m/2$, where m is the mass of the perturbative excitations of the field in the vacuum. For larger frequencies, the power increases but it is cut-off at $w \gg m$. This is due to the destructive interference of the different sections of the string that act as a source of the radiation.

We proceed in a similar manner to compute the radiation from the shape mode excitations. The results indicate that a shape mode on the domain wall string can live for a substantially long time. This could be much longer than the typical time scale of the soliton associated with its width. These results suggest the possibility of obtaining an effective worldsheet action that incorporates the dynamics of these modes in the regime where they do not appreciably radiate.

We start this investigation by considering the effective action for the wiggles on the domain wall string. In the absence of any massive mode we take the Nambu-Goto as the appropriate action. In order to test this action we perform a series of numerical experiments where we compare the results obtained in a lattice field theory evolution with the predictions

from NG. Our results show that, in the regime where the radius of curvature of the domain wall string is large compared to the thickness of the soliton, the position of the string is described perfectly by the NG action.

We then move on to describe the coupling of the shape mode to the NG action. The simplest way to do this is to imagine this excitation as a massive scalar field degree of freedom living on the string worldsheet. Guided by these ideas, we write the action at the lowest order that couples these modes. The presence of this new degree of freedom can affect the dynamics of the domain wall string. We test this idea by looking at the motion of a domain wall loop that naturally collapses under its own tension. We do this in two different ways: we solve the field theory equations for a ring with cylindrical symmetry and compare the results to the ones predicted by our effective action. The results in field theory show that the presence of an excitation can slow down the collapse of the domain wall. This is, indeed, qualitatively captured by the effective action as well. In the effective action one can see this effect as a mechanical backreaction of the excitation on the domain wall. However, it is difficult to go beyond this qualitative comparison due to the presence of radiation in the most interesting cases where the shape mode is more relevant.

Another interesting aspect of this effective theory is the appearance of parametric resonance effects between the internal mode excitation and the wiggles of the domain wall string. The physical origin of this effect is due to the oscillatory behaviour of the effective pressure on the domain wall string due to the scalar field excitations. This is a similar effect to the one in the non-relativistic string discussed long ago [28]. This seems to suggest that this may be a fairly generic effect that could be relevant for other areas of physics where an internal mode changes periodically the equation of state of a soliton. Applications to other effective theories similar to the one presented here could be interesting, for example in the context of braneworlds.

Our numerical investigations of these field theory excited solitons in a lattice show that indeed these parametric resonance effects are present in the full theory. However, a detailed comparison of the results shows that the frequency of the zero mode instability is half of the one predicted in the effective theory.

We have studied this issue from a different perspective with the help of a reduced Lagrangian that describes the coupling between the amplitudes of the different field theory modes on the domain wall strings. This investigation has led us to a Mathieu type equation for the amplitude of a standing wave of the string position. This equation is well known to have regions of instability. This is precisely the instability that we observe in field theory with the correct frequency.

These results suggest that one should include new couplings into the simplest effective theory that we have been discussing. One such term could be a non-minimal coupling

between the massive scalar field and the Ricci scalar of the worldsheet. Looking at the lowest order approximation of the equations of motion obtained from an action including this term, one identifies the existence of the parametric resonances of the form encountered in field theory. This hints to the possibility that indeed this term should be present in the effective theory.

The appearance of these parametric resonances leads to a more rapid decay of the energy stored in the shape mode. This seems to indicate that these excited states would only play a transient role in a cosmological model. However, this conclusion may change if there is any mechanism that would populate these modes later on in the evolution of the defects. In order to investigate this possibility, we have performed a numerical experiment in field theory that mimics the possible excitation of these modes in the late universe. The process assumes the presence of wiggles propagating on the domain wall that, through their collision, could excite the internal modes. This is certainly a possibility. However, our field theory simulations demonstrate that these internal modes are not excited unless the frequency of the wiggles is of the order of the thickness of the string. In other words, long wavelength excitations expected to be present at late times do not seem to have the capacity of populating the internal modes, so we conclude again that internal modes are only relevant for a short cosmological time scale ²⁰.

Finally, let us remark that even though our arguments are very suggestive they are not straightforwardly extrapolated to $(3 + 1)$ dimensions. In the case of strings in $(3 + 1)d$ there are other processes that might be relevant for the possible excitation of the internal modes. In particular, it was suggested in [31] that intercommutation processes (when a loop is formed) could lead to internal excitations. It is hard to see whether this can be enough to significantly affect the evolution of the loop as a whole, but this is something that should be investigated further. Furthermore, even though it seems reasonable to expect that there will also be parametric resonant effects in these models in higher dimensions, this has not been conclusively shown yet. One should therefore use similar numerical techniques to the ones presented in this paper to analyze these possible resonances in models of strings in $(3 + 1)d$. We leave these issues for a future publication.

IX. ACKNOWLEDGEMENTS

We are grateful to Ken Olum, Tanmay Vachaspati and Alex Vilenkin for many useful discussions. This work is supported in part by the Spanish Ministry MCIU/AEI/FEDER grant

²⁰ We should show this explicitly by performing numerical simulations of networks of domain wall strings in field theory. Some effort in this direction is already underway.

PGC2018-094626-B-C21 as well as the PID2021-123703NB-C21 grant funded by MCIN/ AEI /10.13039/501100011033/ and by ERDF; "A way of making Europe", the Basque Government grants (IT-979-16 and IT-1628-22) and the Basque Foundation for Science (IKER-BASQUE). The numerical work carried out in this paper has been possible thanks to the computing infrastructure of the ARINA cluster at the University of the Basque Country, (UPV/EHU).

Appendix A: Details of the numerical calculations

In the following appendix we will describe some of the technical details about the lattice field theory simulations in several different sections of the main paper. Furthermore, we will also give an explicit account of the way one can extract the relevant data to make a precise comparison of the evolution of the domain wall strings with the predictions from the Nambu-Goto action.

In the rest of the section, x will denote the direction perpendicular to the domain wall while y would describe the parallel one. Moreover, we will refer to the length of each side of the simulation box as L_x and L_y (where x, y range from $-L_{x,y}/2$ to $L_{x,y}/2$), and $\Delta x = \Delta y$ and Δt will respectively denote the lattice spacing and time step. The number of points in each dimension is $L_{x,y}/\Delta x$. The numerical values of these scales will be chosen conveniently depending on the particular experiment we want to perform.

1. Lattice simulations

As we describe in the main part of the text, the equation of motion that we are solving throughout this paper can be written in dimensionless form as

$$\frac{\partial^2 \phi}{\partial t^2} - \frac{\partial^2 \phi}{\partial x^2} - \frac{\partial^2 \phi}{\partial y^2} + \phi(\phi^2 - 1) = 0, \quad (\text{A1})$$

where $\phi(t, x, y)$ describes the scalar field living in a $(2 + 1)d$ spacetime. Regarding the boundary conditions, we use absorbing boundary conditions in the x direction (for the details, see the following subsection) and periodic ones in the y direction. Standard discretization techniques were employed for the numerical evolution (staggered leapfrog method and nearest neighbours), and we implemented *message passing interface* (MPI) in our parallelized code in order to handle the large number of lattice points, which is typically of the order of 10^6 .

Let us now briefly discuss some of the specific details relevant for the different simulations we carry out in the sections of the main paper. In what follows, $L_{x,y}$ are to be compared with the dimensionless width of the string, $\delta \sim 1$.

1. In section IIIA we analyze the radiation emitted from small amplitude standing waves in the position of the core of the domain wall. As one can show analytically, when these perturbations couple quadratically to the scattering states, the wavelength of the radiation in the x direction is approximately given by $\lambda_{rad} = 2\pi/\sqrt{4\omega^2 - 2}$, where ω is the angular frequency of the standing wave. For ω sufficiently close to threshold frequency, $m/2 = \sqrt{2}/2$, this wavelength is large, so one needs a big box in the transverse direction in order for the emitted radiation to fit in. Moreover, we are interested in the radiation very far away from the soliton. In our simulations (red points in Fig. 3) we chose $L_x = 200$, which is more than enough to avoid any problems related to the spatial extent of the radiation. On the other hand, we varied L_y from 4 to 26 in order to get the desired frequencies for the standing wave ²¹. Regarding lattice spacing, we used $\Delta x = 0.02, 0.04$ and $\Delta t = 0.005, 0.01$. We ran the simulations for 2×10^5 time steps and found the energy flux accross the lines $x = \pm 98$ at late times. As we will point out in the following subsection, the refinement of the absorbing boundary conditions taking into account the particular frequency of the emitted radiation was crucial in these experiments.

2. For the simulations of travelling wave collisions in section IVA1, we need a large initial separation between wiggles in order for them to be as close as possible to exact Vachaspati-Vachaspati solutions [19]. We evolve the initial configuration Eq. (28) with

$$\psi_+(y+t) = -8 \left[\tanh\left(\frac{y+t-120}{12}\right) - \tanh\left(\frac{y+t-80}{12}\right) \right], \quad (\text{A2})$$

$$\psi_-(y-t) = 8 \left[\tanh\left(\frac{y-t+120}{12}\right) - \tanh\left(\frac{y-t+80}{12}\right) \right]. \quad (\text{A3})$$

The box size and lattice spacing in these simulations were $L_x = 100$, $L_y = 400$ and $\Delta x = 0.1$; $\Delta t = 0.05$. We ran for thousands of time steps in order to let the wiggles collide several times.

These wiggles are quite flat even for big amplitudes, which is convenient because we want to avoid high curvatures that could spoil the comparison with the Nambu-Goto

²¹ Recall that periodic boundary conditions in the y direction force waves on the string to have frequencies given by $2\pi n/L_y$, where n is an integer number.

dynamics. For these particular wiggles, the curvature (i.e., the ratio string thickness to radius of curvature) during interaction is around 0.12 (at most).

3. In the simulations of section VI, the initially excited shape mode triggers the amplification of zero modes with specific frequencies. In order to see this effect, we had to make sure that the size of the box in the y direction was a multiple of the wavelength of the resonant zero modes.

For the experiments in section VIB, we start out with the configuration given in Eq. (40) with $\omega_0 = 2\pi/10$ (which is sufficiently close to the actual resonance frequency, $\omega_s/2$) and a very small amplitude for the zero mode in order to accelerate the appearance of the mode amplification. According to Eq. (42), if this amplitude is set initially to 0, the zero mode should not be amplified. However, numerically the resonance occurs, albeit at very late times. Indeed, numerical inaccuracies are enough to excite the resonance. For these simulations we chose $L_x = L_y = 20$, $\Delta x = 0.01$ and $\Delta t = 0.005$.

In section VIC the field was initialized according to Eq. (46). We performed two groups of simulations corresponding to two different wave numbers for the shape mode: $k_s = 2\pi/3.4$ and $k_s = 2\pi/5$. For each group we took several values for the length of the box in the y direction: $L_y = 17, 34, 51, 68$ for the former and $L_y = 20, 50, 75, 85, 100$ for the latter, with typical lattice spacing of $\Delta x = 0.03$ and time step $\Delta t = 0.01$.

4. Finally, the collisions of travelling wave packets in section VII were simulated in a lattice with $L_x = 32$, $L_y = 800$, $\Delta x = 0.08$ and $\Delta t = 0.02$. The initial state is given by Eq. (28) with

$$\psi_+(y+t) = -\frac{B}{4} \left[\tanh\left(\frac{y+t-220}{25}\right) - \tanh\left(\frac{y+t-180}{25}\right) \right] \cos[\omega(y+t)] , \quad (\text{A4})$$

$$\psi_-(y-t) = \frac{B}{4} \left[\tanh\left(\frac{y-t+220}{25}\right) - \tanh\left(\frac{y-t+180}{25}\right) \right] \cos[\omega(y-t)] . \quad (\text{A5})$$

These are sinusoidal wiggles with amplitude controlled by B and angular frequency ω . We performed three groups of simulations: wiggles with frequency $\omega = 2\pi/20$ (below the resonance frequency), $\omega = 2\pi/10$ (very close to the resonance frequency) and $\omega = 2\pi/5$ (above the resonance frequency). In each case, B was adjusted to get the desired ratio of the thickness of the soliton to the radius of curvature of the order of 0.1.

We performed a convergence test to show the robustness of the results presented in that section, specifically in Fig. 13. Simulations with 10^6 , 4×10^6 and 1.6×10^7 lattice points and $\Delta x = 0.16, 0.08$ and 0.04 , respectively, give almost identical results.

2. Tuned Absorbing boundary conditions

As previously stated, we have implemented absorbing boundary conditions in the x direction. This is because an important part of the radiation produced in our simulations is emitted along that direction. Implementing these absorbing boundary conditions allows us to run for very long periods of time without having to worry about the effects of the radiation bouncing off the walls and re-exciting the soliton.

Let us briefly discuss the reasoning behind these specific boundary conditions we use. In order to do that, we first note that far away from the soliton (in the $x \rightarrow \pm\infty$ limit) we can assume that the field is described as a perturbation around the vacuum of the form $\phi_{\pm}(x, y, t) = \pm 1 + \xi_{\pm}(x, y, t)$. At the linear level, the equation of motion yields a solution for this perturbation as a travelling wave, $\xi_{\pm}(x, y, t) \propto \cos(\omega_r t \mp k_x x \mp k_y y + \delta)$ with $\omega_r = \sqrt{k_x^2 + k_y^2 + 2}$ (recall that the dimensionless mass is $\sqrt{2}$). Assuming normal incidence (i.e., $k_y = 0$), this wave is a solution to the so-called Mur boundary conditions [32],

$$\left. \frac{\partial \phi}{\partial t} \pm \frac{\partial \phi}{\partial x} \right|_{x=\pm L_x/2} = 0, \quad (\text{A6})$$

if $\omega_r = k_x$. Therefore, these conditions are efficient at absorbing waves with $k_x \gg m$.

One can refine the Mur boundary conditions for monochromatic radiation with known angular frequency ω_r by using instead

$$\left. \frac{\partial \phi}{\partial t} \pm \frac{\omega_r}{\sqrt{\omega_r^2 - m^2}} \frac{\partial \phi}{\partial x} \right|_{x=\pm L_x/2} = 0. \quad (\text{A7})$$

As one can easily check, the travelling waves ξ_{\pm} above are exact solutions to these equations. This tuning of the absorbing boundary conditions turned out to be crucial in our simulations, specially in those of section III, where we knew the angular frequency of the outgoing radiation: $\omega_r = 2\omega$. Here, ω is the frequency of the zero mode that couples to the scattering states. Note that (A6) and (A7) are nearly equivalent if $\omega_r \gg m$, or $\omega \gg m/2$. However, this may not be the case as we are free to choose the angular frequency of the zero mode to be arbitrarily close to $m/2$. We employed the refined boundary conditions (A7) for the standing wave experiments in sections III and IV, and the version (A6) for the rest.

3. Nambu-Goto reconstruction of a field theory domain wall

In this appendix we would like to outline the main steps required to obtain a Nambu-Goto description of a domain wall string that has been simulated in a lattice field theory²². The starting point for this reconstruction is to obtain the data points for the position of the domain wall for the particular time step that we are interested in. We do this in our lattice by identifying the spatial coordinates on the (x, y) plane where the field goes to zero. This is our definition of the position of the domain wall.

In order to subsequently obtain the velocity of the domain wall string we actually need two data lists containing the spatial coordinates of the domain wall at $t = 0$ and $t = \Delta t$:

- *String 1*: list of N vectors \vec{r}_n^0 , with $n = 0, 1, \dots, N - 1$, corresponding to the positions of every point on the domain wall string at $t = 0$.
- *String 2*: list of M vectors \tilde{r}_m^0 , with $m = 0, 1, \dots, M - 1$, corresponding to the positions of every point on the domain wall string at $t = \Delta t$.

The Nambu-Goto reconstruction algorithm consists of the following steps:

a. Computing tangent vectors

The first step is to find the N vectors \vec{r}_n^t which are tangent to *String 1* at each point n . For $n = 0$ to $n = N - 1$, we define the tangent vectors

$$\vec{r}_n^t = \vec{r}_{n+1} - \vec{r}_n, \tag{A8}$$

where $\vec{r}_N = \vec{r}_0 + L_y \hat{j}$. Here, \hat{j} denotes the unitary vector in the y direction. We will also need the unit tangent vectors, namely

$$\hat{r}_n^t = \frac{\vec{r}_{n+1} - \vec{r}_n}{|\vec{r}_{n+1} - \vec{r}_n|}. \tag{A9}$$

b. Nambu-Goto velocity and Lorentz factor

Consider a particular point n on *String 1*. Let us call this point P . In order to find its velocity, we have to identify it with a point P_* on *String 2* (note that, in general, the point P_* we want to find is not exactly one of the M vectors found in the first step of the algorithm). Since in the conformal gauge in NG the velocity of P is perpendicular to \vec{r}_n^t ,

²² Here we use the term Nambu-Goto to mean that we can parametrize the domain wall string with the usual conformal gauge in a Nambu-Goto description (see section IV for more details).

P_* is the intersection of *String 2* with the plane Π_n perpendicular to \vec{r}_n^t at P . Let q and $q + 1$ be the labels of the two points on *String 2* (with position vectors \vec{r}_q and \vec{r}_{q+1}) which are closer to Π_n . If they are in opposite sides of the plane, P_* is the intersection of Π_n with the line that contains both points q and $q + 1$.

Once we have found the point P_* on *String 2* which corresponds to \vec{r}_n on *String 1*, we can compute the Nambu-Goto velocity as

$$\dot{\vec{r}}_n^{NG} = \frac{\vec{r}_* - \vec{r}_n}{\Delta t}, \quad (\text{A10})$$

and the Lorentz factor as

$$\Gamma_n = \frac{1}{\sqrt{1 - |\dot{\vec{r}}_n^{NG}|^2}}. \quad (\text{A11})$$

c. Amount of σ parameter in each string segment

The gauge we are working in imposes the following condition:

$$\dot{\vec{r}}_n^{NG\ 2} + \vec{r}_n'^2 = 1, \quad (\text{A12})$$

where the prime denotes derivative with respect to σ (see beginning of section IV). Therefore, $|\vec{r}_n'| = |\vec{r}_n^t|/\Delta\sigma_n = \sqrt{1 - \dot{\vec{r}}_n^{NG\ 2}}$, which yields

$$\Delta\sigma_n = \Gamma_n |\vec{r}_n^t|, \quad (\text{A13})$$

which gives the amount of energy (or amount of parameter σ) in this section of the string.

d. Redefinition of the tangent vectors

Now, we simply redefine the tangent vectors according to their correct parametrization in our gauge in the following way:

$$\vec{r}_n^{tNG} = \frac{\hat{\vec{r}}_n^t}{\Gamma_n}. \quad (\text{A14})$$

e. Left and right movers: $\vec{a}(\sigma)$ and $\vec{b}(\sigma)$

With the Nambu-Goto velocities (A10) and the new Nambu-Goto tangent vectors (A14), we can find the vectors

$$\begin{cases} \vec{a}'_n = \vec{r}_n^{tNG} - \dot{\vec{r}}_n^{NG}, \\ \vec{b}'_n = \vec{r}_n^{tNG} + \dot{\vec{r}}_n^{NG}. \end{cases} \quad (\text{A15})$$

Moreover, as we also know the amount of sigma parameter $\Delta\sigma_n$ in each string segment, we can obtain the correct parametrization of $\vec{a}(\sigma)$ and $\vec{b}(\sigma)$. This is, in fact, all the information we need to reconstruct the evolution of the string at any moment in time. We have used this algorithm to obtain the motion of the domain wall string in section IV.

Finally, let us comment on the reconstructed NG energy. At each time step, the energy of the string can be computed as

$$E = \sum_{n=0}^{N-1} \Delta\sigma_n = \sum_{n=0}^{N-1} \Gamma_n |\vec{r}_n^t|, \quad (\text{A16})$$

where we have set the string tension $\mu = 1$. If the string moves according to the NG action, E is conserved. Let us label our lattice field theory files as $1, 2, \dots, T$, where T is the total number of time steps. One can calculate the quantity (A16) taking these files in pairs (Γ_n contains the velocities of each point, and the computation of the velocities requires two time steps) to obtain the NG energy at every time step in the field theory simulation: E_1, E_2, \dots, E_{T-1} . Here, E_j is the energy of the string computed from files j and $j+1$. If these energies are different from each other, the string is not behaving as the NG action predicts.

Appendix B: The scalar field ansatz for Nambu-Goto dynamics

In many instances, one would like to have an expression for the scalar field in our model that accurately represents a domain wall moving according to the Nambu-Goto dynamics. Here, we use the knowledge of several examples where these solutions are known exactly to motivate a scalar field ansatz that approximately parametrizes the scalar field theory configuration from a generic solution of the Nambu-Goto dynamics.

Let's start by describing the static field theory configuration of the domain wall centered around the $x = x_0$ point and extended in the y direction, namely the solution

$$\phi_s(x, y, t) = \phi_K(x - x_0). \quad (\text{B1})$$

It is well known that one can obtain a new exact solution describing a domain wall moving at a constant velocity (v) by writing

$$\phi_b(x, y, t) = \phi_K\left(\frac{x - (x_0 + vt)}{\sqrt{1 - v^2}}\right). \quad (\text{B2})$$

This is obviously an exact solution since it can be obtained by boosting the original solution to a frame moving with velocity v .

Let us now consider another type of solution where the domain wall is not completely aligned with the y axis but is slightly inclined with respect to it. The solution for the static configuration of this kind would be given by

$$\phi_{\Theta}(x, y, t) = \phi_K((x - x_0) \cos \Theta - y \sin \Theta) = \phi_K\left(\frac{x - (x_0 + y \tan \Theta)}{\sqrt{1 + \tan^2 \Theta}}\right). \quad (\text{B3})$$

This is nothing but the same static configuration obtained earlier but now rotated by an angle Θ . In the last expression the argument of the field ϕ_K has been expressed in a particular way for reasons that will become apparent immediately.

Both these types of solutions given in Eqs (B2) and (B3) are exact solutions of the equations of motion and can be collectively described by a single expression of the form

$$\phi(x, y, t) = \phi_K\left(\frac{x - \psi(y, t)}{\sqrt{1 + \dot{\psi}^2 - \dot{\psi}^2}}\right), \quad (\text{B4})$$

if we take $\psi_b(y, t) = x_0 + vt$ for the boosted domain wall case and $\psi_{\Theta}(y, t) = x_0 + y \tan \Theta$ for the wall with an angle.

Moreover, we also notice that taking this ansatz for the scalar field with the extra condition that $\dot{\psi}^2 = \dot{\psi}^2$ one identifies the exact expression for the Vachaspati-Vachaspati travelling wave solutions described in [19].

All these arguments strongly suggest that this type of ansatz could be a good description for a generic motion of the string. Therefore, we consider the ansatz

$$\phi(x, y, t) = \phi_K\left(\frac{x - \psi(y, t)}{\sqrt{1 - \partial_a \psi \partial^a \psi}}\right), \quad (\text{B5})$$

where we have introduced the relativistic notation for the coordinates along the string world-sheet, namely $a = t, y$.

Guided by these considerations, we decided to study the effective action for the field $\psi(y, t)$ in our model by plugging this expression into the original $3d$ scalar field action. Doing this exercise, one arrives to an action of the form

$$S_{\text{effective}} = -\mu \int dt dy \sqrt{1 - \partial_a \psi \partial^a \psi} + \dots, \quad (\text{B6})$$

where the extra terms are proportional to higher order derivatives of the field $\psi(y, t)$. This is exactly the Nambu-Goto action for the dynamics of the perturbations transverse to a domain wall extended along the y direction.

This demonstrates that our field theory ansatz should be an accurate description for the full dynamics of the model as long as the field $\psi(y, t)$ obeys the Nambu-Goto dynamics and one can neglect the higher order terms (curvature terms) and of course any source of radiation.

Finally, note that using this ansatz for the kink solution in 1 + 1 dimensions one recovers the effective action for a relativistic particle dynamics. This could be interesting in models that try to describe the motion of the kink with the use of the collective coordinate language.

Appendix C: Computing the radiation from domain wall excitations

1. Analytic calculation of the radiation from zero mode excitations

Let us consider the following scalar field configuration:

$$\phi(t, x, y) = \phi_K \left[\frac{x - \psi_0(t, y)}{\sqrt{1 - \partial_\mu \psi_0 \partial^\mu \psi_0}} \right] + R(t, x, y), \quad (\text{C1})$$

where ϕ_K is the static domain wall solution, $R(t, x, y)$ denotes collectively the radiation modes and $\psi_0(t, y)$ denotes a zero mode of frequency ω_0 whose expression is given by

$$\psi_0(t, y) = \hat{D}(t) \cos(\omega_0 t) \cos(\omega_0 y). \quad (\text{C2})$$

If we substitute (C1) into the field equation (A1) we obtain, at second order in the amplitude $\hat{D}(t)$, the following equation for the radiation modes:

$$\square R + (3\phi_K^2 - 1) R = -\frac{1}{\sqrt{2}} \hat{D}^2 \omega_0^4 x \operatorname{sech}^2 \left(\frac{x}{\sqrt{2}} \right) (\cos(2\omega_0 t) + \cos(2\omega_0 y)). \quad (\text{C3})$$

In order to obtain the expression (C3) we have kept only linear terms in $R(t, x, y)$, since the radiation has a quadratic source in $\hat{D}(t)$. The response of $R(t, x, y)$ to the time independent term in the inhomogeneous part of (C3) will be itself time independent and it will carry no energy. We may therefore consider the time dependent part as source term for radiation and apply the Green's function method [4, 20] to obtain an asymptotic expression for $R(t, x, y)$ whose form is

$$R = \frac{\hat{D}^2 \pi \omega_0^4 q \operatorname{csch} \left(\frac{\pi q}{2} \right)}{2\sqrt{q^4 + 5q^2 + 4}} \cos \left(\omega t - \frac{qx}{\sqrt{2}} - \tan^{-1} \left(\frac{3q}{q^2 - 2} \right) \right), \quad (\text{C4})$$

where

$$\omega = 2\omega_0, \quad q = \sqrt{2\omega^2 - 4}. \quad (\text{C5})$$

The averaged radiated power per unit length at infinity in the x -direction can be obtained from the energy-momentum tensor:

$$\frac{\langle \dot{E} \rangle}{L_y} = \frac{\langle T_{0x} \rangle}{L_y} = -\frac{\hat{D}^4 \pi^2 \omega_0^9 q^3 \operatorname{csch}^2 \left(\frac{\pi q}{2} \right)}{4\sqrt{2} (q^4 + 5q^2 + 4)}. \quad (\text{C6})$$

where L_y denotes the length of the domain wall string along the extended direction.

On the other hand, the total energy at quadratic order in \hat{D} for a field configuration of the form (C1) is the following:

$$E(t) = M_{DW} + \frac{\sqrt{2}}{6}\omega_0^2 L_y \hat{D}^2(t) + \mathcal{O}(\hat{D}^3(t)), \quad (\text{C7})$$

where $M_{DW} = \sqrt{\frac{8}{9}}L_y$ is the mass of the static domain wall solution. If we assume that all the energy radiated to infinity comes from the zero mode, we obtain the following relation:

$$\frac{dE(t)}{dt} = \langle \dot{E} \rangle, \quad (\text{C8})$$

and therefore,

$$\frac{\sqrt{2}}{3}\omega_0^2 \frac{d}{dt} \hat{D}^2(t) = -\frac{\pi^2 \omega_0^9 q^3 \text{csch}^2\left(\frac{\pi q}{2}\right)}{4\sqrt{2}(q^4 + 5q^2 + 4)} \hat{D}^4(t) \equiv -\alpha(\omega_0) \hat{D}^4(t), \quad (\text{C9})$$

which can be integrated to give

$$\hat{D}(t) = \frac{1}{\sqrt{\frac{1}{\hat{D}^2(0)} + \frac{3\alpha(\omega_0)}{\sqrt{2}\omega_0^2}t}}. \quad (\text{C10})$$

2. Analytic calculation of the radiation from the internal mode excitations

We follow a similar procedure to that of Appendix C 1 to obtain the radiation emitted by the domain wall string shape modes. Let us consider the following ansatz:

$$\phi(t, x, y) = \phi_K(x) + \hat{A} \cos(\omega t) f_1(x) \cos(ky) + R(t, x, y), \quad (\text{C11})$$

where $R(t, x, y)$ corresponds to the radiation modes, $f_1(x)$ is the shape mode profile and k is the frequency of the mode in the longitudinal direction. At second order in \hat{A} we obtain the following equation for the radiation:

$$\begin{aligned} \square R + (3\phi_K^2 - 1)R &= -3\phi_K \hat{A}^2 f_1^2 \cos^2(\omega t) \cos^2(ky) = \\ &= -\frac{3}{4}\phi_K \hat{A}^2 f_1^2 \cos(2\omega t) \cos(2ky) - \frac{3}{4}\phi_K \hat{A}^2 f_1^2 \cos(2\omega t) + (\text{time independent terms}), \end{aligned} \quad (\text{C12})$$

where $\omega = \sqrt{\omega_s^2 + k^2}$ and $\omega_s = \sqrt{3/2}$. As we have mentioned, the response of the radiation to time independent sources is itself time independent and therefore does not carry away radiation. The time dependent term suggests the following form of radiation at infinity:

$$R(t, x, y) = R_1(x) \cos(2\omega t) + R_2(x) \cos(2\omega t) \cos(2ky). \quad (\text{C13})$$

Now, (C12) is satisfied for the ansatz (C13) if the following equations are satisfied simultaneously:

$$-R_1''(x) + (3\phi_K^2 - 1 - (2\omega)^2) R_1 = -\frac{3}{4}\phi_K \hat{A}^2 f_1^2, \quad (\text{C14})$$

$$-R_2''(x) + (3\phi_K^2 - 1 - (2\omega_s)^2) R_2 = -\frac{3}{4}\phi_K \hat{A}^2 f_1^2. \quad (\text{C15})$$

The radiation at infinity may be obtained with the Green's function method [4, 20]. For R_2 we get

$$R_2(t, x, y) = \frac{3}{16}\sqrt{3}\pi \hat{A}^2 \text{csch}\left(\sqrt{2}\pi\right) \cos\left(\sqrt{6}t - 2x - \tan^{-1}\left(\sqrt{2}\right)\right) \cos(2ky). \quad (\text{C16})$$

For R_1 we get

$$R_1(t, x, y) = \frac{3\pi \hat{A}^2 q (q^2 - 2) (q^2 + 4) \text{csch}\left(\frac{\pi q}{2}\right) \cos\left(-\tan^{-1}\left(\frac{3q}{2-q^2}\right) + \frac{qx}{\sqrt{2}} - t\bar{\omega}\right)}{128\sqrt{2}\sqrt{q^4 + 5q^2 + 4}}, \quad (\text{C17})$$

where $q = \sqrt{2\bar{\omega}^2 - 4}$ and $\bar{\omega} = 2\omega$. The averaged radiated power per unit length at infinity in the x -direction can be obtained again from the energy-momentum tensor,

$$\langle T_{0x} \rangle = \langle (\partial_t R_1 + \partial_t R_2) (\partial_x R_1 + \partial_x R_2) \rangle_{t,y}. \quad (\text{C18})$$

Note that for $k = 0$ we recover the standard expression of the averaged radiated power per unit length at infinity $\langle T_{0x} \rangle = \langle T_{0x}^{(\text{kink})} \rangle$, (see [4, 20]). For $k \neq 0$ the cross terms in (C18) are eliminated by the average in the y -direction, reducing the averaged radiated power to the following expression:

$$\langle T_{0x} \rangle = \langle \partial_t R_1 \partial_x R_1 + \partial_t R_2 \partial_x R_2 \rangle_t \equiv T_1 + T_2. \quad (\text{C19})$$

The expression for T_2 does not depend on the frequency in the longitudinal direction and can be related to the averaged power of the standard kink as follows:

$$T_2 = \frac{1}{8} T_{0x}^{(\text{kink})} = -\frac{27}{128} \sqrt{\frac{3}{2}} \pi^2 \hat{A}^4 \text{csch}^2\left(\sqrt{2}\pi\right) = -0.0014 \hat{A}^4. \quad (\text{C20})$$

On the other hand, T_1 does depend on the longitudinal frequency. A similar calculation shows that

$$T_1 = -\frac{9\pi^2 \hat{A}^4 q^3 (q^2 - 2)^2 (q^2 + 4)^3 \text{csch}^2\left(\frac{\pi q}{2}\right)}{65536\sqrt{2} (q^4 + 5q^2 + 4)}. \quad (\text{C21})$$

Finally, taking into account (C8), we can relate the rate of the energy loss of the shape modes with the radiated power at infinity:

$$\frac{1}{2} \left(\frac{3}{2} + k^2 \right) \frac{d}{dt} \hat{A}^2(t) = (T_1 + T_2) \hat{A}^4(t), \quad (\text{C22})$$

which after integration gives

$$\hat{A}(t) = \frac{1}{\sqrt{\frac{1}{\hat{A}^2(0)} + \frac{2(T_1 + T_2)}{\omega_s^2} t}}. \quad (\text{C23})$$

Appendix D: The Lagrangian for the interacting mode amplitudes

In this section we will study the interaction between zero modes and internal modes. The general domain wall solution with periodic boundary conditions in the y -direction in the box $\mathbb{R} \times [-L_y/2, L_y/2]$ can be expanded in the basis of linearized modes as follows:

$$\begin{aligned} \phi(t, x, y) = & \phi_K(x) + \sum_{k=0}^{\infty} D_k(t) f_0(x) \cos(\omega_0(k)y) + \\ & + \sum_{k=0}^{\infty} A_k(t) f_1(x) \cos(\omega(k)y) + R(t, x, y), \end{aligned} \quad (\text{D1})$$

where

$$\omega_0(k) = \frac{2\pi k}{L_y}, \quad \omega(k) = \sqrt{\omega_s^2 + \left(\frac{2\pi k}{L_y}\right)^2}, \quad (\text{D2})$$

and $R(t, x, y)$ stands for the radiation modes. The ansatz (D1) contains all the degrees of freedom and as a consequence, is a general solution of the field equations in the frame of the domain wall.

Let us assume now that the relevant degrees of freedom of the system are given by the zero mode and the homogeneous shape mode (i.e. the shape mode with $k = 0$). We consider the following ansatz:

$$\phi(t, x, y) = \phi_K(x) + A(t) f_1(x) + D(t) f_0(x) \cos(\omega_0 y). \quad (\text{D3})$$

This choice of ansatz implicitly assumes that the radiation does not play any relevant role during the mode interaction. After a proper rescaling of the domain wall action we may substitute (D3) into (1). Integration in the x, y -directions gives the following effective mechanical Lagrangian with two degrees of freedom:

$$\begin{aligned} \frac{2}{L_y} \mathcal{L}_{\text{effec}} = & -\frac{4\sqrt{2}}{3} + \dot{A}^2(t) - \frac{3}{2} A^2(t) + \frac{1}{2} \dot{D}^2(t) - \frac{1}{2} \omega_0^2 D^2(t) - \frac{3}{2} C_1 A^2(t) D^2(t) \\ & - \frac{3}{4} C_1 A^4(t) - \frac{9}{16} C_1 D^4(t) - 3C_2 A(t) D^2(t) - 4C_2 A^3(t), \end{aligned} \quad (\text{D4})$$

where $C_1 = 3\sqrt{2}/35$ and $C_2 = 3\sqrt{3}\pi/(64 \cdot 2^{3/4})$. The equations of motion for $A(t)$ and $D(t)$ are therefore

$$\ddot{A}(t) + \frac{3}{2} [1 + C_1 D^2(t)] A(t) + 6C_2 A^2(t) + \frac{3C_1}{2} A^3(t) + \frac{3C_2}{2} D^2(t) = 0, \quad (\text{D5})$$

$$\ddot{D}(t) + [\omega_0^2 + 6C_2 A(t) + 3C_1 A^2(t)] D(t) + \frac{9C_1}{4} D^3(t) = 0. \quad (\text{D6})$$

Let us assume first that the shape mode is initially excited. At first order we have

$$A(t) = \hat{A} \cos(\omega_s t). \quad (\text{D7})$$

In the background of this solution and assuming that $A(t)$ and $D(t)$ are small, the field equation for $D(t)$ takes approximately the following form:

$$\ddot{D}(t) + \left(\omega_0^2 + 6C_2 \hat{A} \cos(\omega_s t) \right) D(t) = 0. \quad (\text{D8})$$

This is nothing but a Mathieu equation (see Appendix E). It is well-known that this equation has instabilities for some relations between ω_0 , ω_s and \hat{A} . As we will explain later, in our case this translates into the condition $\omega_0 \approx \frac{\omega_s}{2}$. At this point, one expects an exponential growth in the amplitude of the zero mode.

On the other hand, if one assumes that the zero mode is initially excited,

$$D(t) = \hat{D} \cos(\omega_0 t), \quad (\text{D9})$$

then for initially small $D(t)$ and $A(t)$ the equation for the shape mode is

$$\ddot{A}(t) + \frac{3}{2}A(t) + \frac{3C_2}{2}\hat{D}^2 \cos^2(\omega_0 t) = 0. \quad (\text{D10})$$

This is the equation of the forced harmonic oscillator whose resonance will occur at $\omega_0 = \omega_s/2 = \sqrt{3/2}/2$. In a realistic situation both modes are coupled, allowing for an energy transfer between them. As we have explained in Sec. VIB, this coupling prevents the amplitudes $A(t)$ or $D(t)$ to grow indefinitely.

Let us take now the following initial configuration:

$$\phi(t, x, y) = \phi_K(x) + A(t)f_1(x) \cos(k_s y) + D_1(t)f_0(x) \cos(k_1 y) + D_2(t)f_0(x) \cos(k_2 y), \quad (\text{D11})$$

i.e. the shape mode may have now a frequency k_s in the y -direction, and two zero modes with different frequencies k_1 and k_2 are allowed. Repeating the same process as before we obtain the following mechanical Lagrangian:

$$\begin{aligned} \frac{2}{L_y} \mathcal{L}_{\text{effec}} = & -\frac{4\sqrt{2}}{3} + \frac{1}{2}\dot{A}^2(t) + \frac{1}{2}\dot{D}_1^2(t) + \frac{1}{2}\dot{D}_2^2(t) - \frac{1}{2}(\omega_s^2 + k_s^2)A^2(t) - \\ & -\frac{1}{2}k_1^2 D_1^2(t) - \frac{1}{2}k_2^2 D_2^2(t) - C_3 \left(\frac{1}{2}A^4(t) + D_1^4(t) + D_2^4(t) \right) - \\ & -\frac{3}{4}C_1 (A^2(t)D_1^2(t) + A^2(t)D_2^2(t) + 3D_1^2(t)D_2^2(t)) - 3C_2 A(t)D_1(t)D_2(t), \end{aligned} \quad (\text{D12})$$

where $C_3 = 27/(280\sqrt{2})$. The field equations at quadratic order are

$$\ddot{A}(t) + [\omega_s^2 + k_s^2] A(t) + 3C_2 D_1(t)D_2(t) = 0, \quad (\text{D13})$$

$$\ddot{D}_1(t) + k_1^2 D_1(t) + 3C_2 A(t)D_2(t) = 0, \quad (\text{D14})$$

$$\ddot{D}_2(t) + k_2^2 D_2(t) + 3C_2 A(t)D_1(t) = 0. \quad (\text{D15})$$

We have obtained the Lagrangian and field equations assuming that $k_1 \neq k_s/2$, $k_2 \neq k_s/2$ and $|k_1 - k_2| = k_s$. When the three conditions are met, it is possible for a shape mode with frequency k_s in the y -direction to excite a couple of zero modes of frequencies k_1 and k_2 if, in addition, the condition $k_1 + k_2 = \sqrt{3/2 + k_s^2}$ holds. For details in the study of these types of instabilities we refer to [30]. We show in the main part of the text how one can find examples of these parametric resonances in multiple modes in our field theory simulations of the domain wall string. The results are in perfect agreement with the conclusions obtained from these equations.

Appendix E: Brief review of the Mathieu equation

The standard form of the Mathieu equation is given by

$$\ddot{x}(t) + (a - 2q \cos(2t)) x(t) = 0. \quad (\text{E1})$$

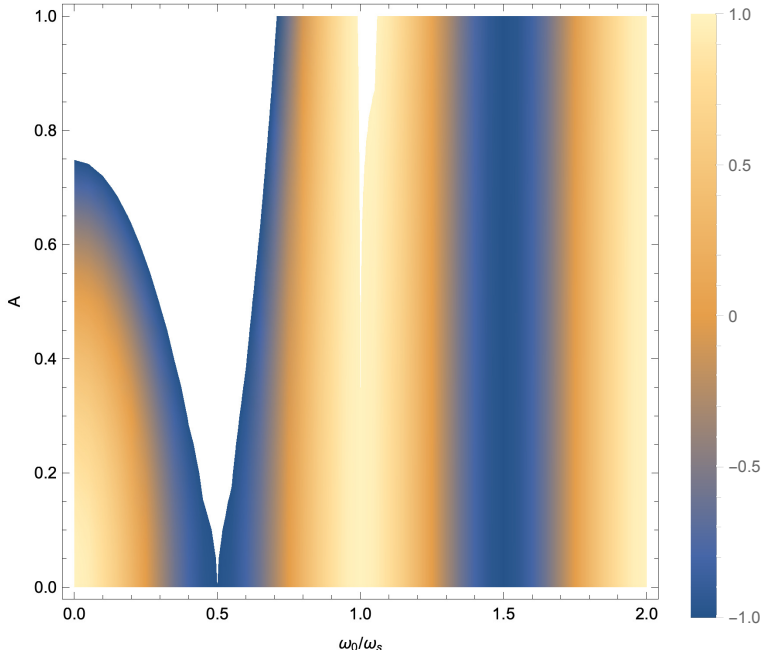


FIG. 14: Stability/instability regions of (D8). The white band represents the unstable region. The color palette indicates the trace of the monodromy matrix, Δ . For $|\Delta| < 1$ the solutions of the Mathieu equations are stable. For details see [29].

It is well-known that this equation has unstable solutions in some regions of the parameter space (a, q) , which are characterized in terms of the trace of the monodromy matrix of the associated first order system. Note that (E1) can be brought to the form (D8) after the

following identifications:

$$x \rightarrow D, \quad t = \frac{\omega_s}{2} t', \quad a = \frac{4\omega_0}{\omega_s^2}, \quad \text{and} \quad q = -\frac{12C_2\hat{A}}{\omega_s^2}. \quad (\text{E2})$$

Using standard results in Floquet analysis, it can be shown that for small \hat{A} the unstable regions satisfy the relation $\omega_0/\omega_s = k/2$, with k a natural number. As \hat{A} increases, the unstable band gets wider, and therefore the number of unstable frequencies grows with \hat{A} . On the other hand, as k increases, the unstable region gets narrower. As a consequence, to excite higher unstable frequencies one needs values of the amplitude \hat{A} above the linear level. The regions of instability for Eq. (D8) can be read from Fig. 14. For details in the analysis of Mathieu equations see [29].

Appendix F: Parametric instability due to higher order corrections in the effective action

In this appendix we show that a term of the form (53) added to the effective action (35) is able to explain the parametric resonance of a zero mode with half the frequency of the homogeneous internal excitation, as observed in our lattice field theory simulations.

Supplemented with a coupling between the scalar field θ representing the amplitude of the shape mode and the Ricci scalar \mathcal{R} associated with the induced metric on the string worldsheet, the effective action reads

$$S = \int d^2\xi \sqrt{-\gamma} \left[(\alpha + \beta\theta) \mathcal{R} - \mu + \frac{1}{2} \gamma^{ab} \partial_a \theta \partial_b \theta - V(\theta) \right], \quad (\text{F1})$$

where α and β are real constants and $V(\theta) = \frac{1}{2} m_\theta^2 \theta^2 + \mathcal{O}(\theta^3)$, with $m_\theta = \omega_s$. Varying this action with respect to the coordinates of the string position, $X^\mu(\xi^0, \xi^1)$, we get the following equations of motion:

$$\partial_b \left[\sqrt{-\gamma} (M^{ab} - 2\beta F^{ab}) \partial_a X^\mu \right] = 0, \quad (\text{F2})$$

where the symmetric tensors M^{ab} and F^{ab} are given by

$$M^{ab} = 2(\alpha + \beta\theta) G^{ab} + \mu \gamma^{ab} + T^{ab}, \quad (\text{F3})$$

$$F^{ab} = \gamma^{ac} \gamma^{bd} \nabla_c \nabla_d \theta - \gamma^{ab} \nabla_c (\gamma^{cd} \nabla_d \theta). \quad (\text{F4})$$

On the one hand, $G^{ab} = R^{ab} - \frac{1}{2} \gamma^{ab} \mathcal{R}$ in Eq. (F3) is the Einstein tensor, which vanishes in 1 + 1 dimensions. On the other hand, T^{ab} is the energy-momentum tensor of the scalar field: $T^{ab} = \gamma^{ab} V(\theta) - \frac{1}{2} \gamma^{ab} \gamma^{cd} \partial_c \theta \partial_d \theta + \gamma^{ac} \gamma^{bd} \partial_c \theta \partial_d \theta$.

Assuming that θ is only a function of time, the expansion of Eq. (F2) for $X^1 = \psi(t, y)$ to lowest order in θ and ψ reads

$$\ddot{\psi} - \left(1 + \frac{2\beta}{\mu}\ddot{\theta}\right)\psi = 0. \quad (\text{F5})$$

Finally, using the approximation $\theta(t) = \theta_0 \cos(\omega_s t)$ and assuming that $\psi(t, y) = D(t) \cos(\omega_0 y)$, we find a Mathieu equation for the amplitude of the zero mode:

$$\ddot{D}(t) + \omega_0^2 \left[1 - \frac{2\beta\omega_s^2}{\mu}\theta_0 \cos(\omega_s t)\right] D(t) = 0. \quad (\text{F6})$$

Therefore, amplification occurs for waves of frequency $\omega_0 = \omega_s/2$.

Appendix G: Domain wall ring collapse

In our discussion on the effective action describing the internal mode excitation of a domain wall string, we argued that one can think of the amplitude of this mode as a massive scalar field living on the worldsheet of the soliton. Therefore, it seems natural to propose a covariant version of the effective action for this mode in a generic string configuration as

$$S = \int d^2\xi \sqrt{-\gamma} \left[-\mu + \frac{1}{2}\gamma^{\alpha\beta}\partial_\alpha\theta\partial_\beta\theta - \frac{1}{2}m_\theta^2\theta^2 \right], \quad (\text{G1})$$

where the first term gives the Nambu-Goto action, while the other two terms describe the evolution of the internal mode and its coupling to the Goldstone modes encoded on the induced metric γ .

Here we will be interested in studying the motion of a circular loop parametrized by the spacetime position

$$X^\mu(t, \tilde{\sigma}) = (t, R(t) \cos(\tilde{\sigma}/R_0), R(t) \sin(\tilde{\sigma}/R_0)). \quad (\text{G2})$$

Without any excitation, or in other words, with $\theta = 0$ everywhere in the loop, the previous action will yield the equation

$$\dot{R}^2 = 1 - \left(\frac{R}{R_0}\right)^2, \quad (\text{G3})$$

whose solution for a static initial configuration with $R(t=0) = R_0$ is given by

$$R(t) = R_0 \cos\left(\frac{t}{R_0}\right). \quad (\text{G4})$$

This represents the evolution of a static ring that collapses under its own tension in a time $t_c = \pi R_0/2$.

Let us now consider the case of a ring with some extra energy due to the presence of an excited internal mode. In our language, this means that we will start with an initial condition with $\theta(t = 0) = \theta_*$.

The equations of motion in this case become

$$\begin{aligned} \ddot{R}(t) &= -\frac{(1 - \dot{R}^2)}{R} \times \left[\frac{1}{F(\theta) + \frac{\dot{\theta}^2}{2\mu} \frac{1+2\dot{R}^2}{1-\dot{R}^2}} \left(F(\theta) + \frac{1}{2\mu} \dot{\theta}^2 \left(\frac{2\dot{R}^2 - 1}{1 - \dot{R}^2} \right) + \frac{R\dot{R}\dot{\theta}}{\mu} \left(\frac{\ddot{\theta}}{1 - \dot{R}^2} + m_\theta^2 \theta \right) \right) \right], \\ \ddot{\theta} + \dot{\theta} \frac{\dot{R}}{R} \left(1 + \frac{R\ddot{R}}{1 - \dot{R}^2} \right) + (1 - \dot{R}^2) m_\theta^2 \theta &= 0, \end{aligned} \tag{G5}$$

where

$$F(\theta) = \left(1 + \theta^2 \frac{m_\theta^2}{2\mu} \right). \tag{G6}$$

These equations are quite complicated, so we will need to solve them numerically. However, there are a few effects that are worth noticing since they could be qualitatively important.

We first note that the equation of motion for the radius of the loop gets corrected by the presence of the scalar field amplitude $\theta(t)$ through the factor included within large brackets in the equation for $R(t)$ in Eq. (G5). In fact, it can be shown that for time scales larger than the period of oscillation of the scalar field, this correction decreases the collapsing force on the ring. This is however difficult to test since this effect becomes relevant only for large amplitude configurations for $\theta(t)$, but it is exactly in these cases where radiation becomes important and this mechanism of energy loss is not present in our equations above.

Another important effect can be seen in the equation for the scalar field θ . In a collapsing ring, the second term proportional to $\dot{\theta} \frac{\dot{R}}{R}$ induces an anti-friction effect that drives the scalar field to larger amplitudes. This will increase the amount of energy in the excited mode. However, the collapsing loop also increases its energy per unit length due to the increase of kinetic energy, so the overall effect is not so dramatic as one might think.

In order to test the validity of these equations we have implemented a field theory simulation that reproduces this collapse from an approximate initial condition. Here we take advantage of the symmetry of the problem and solve the equations of motion in the $1 + 1$ description in terms of the radial coordinate. We take the initial radius of the domain wall loop to be very large compared to its thickness. This allows us to use the static field configuration for the kink centered at this radius as a pretty accurate approximation for the initial state²³.

²³ We take an absorbing boundary condition at infinity and a vanishing value of the derivative of the field at the center of the loop.

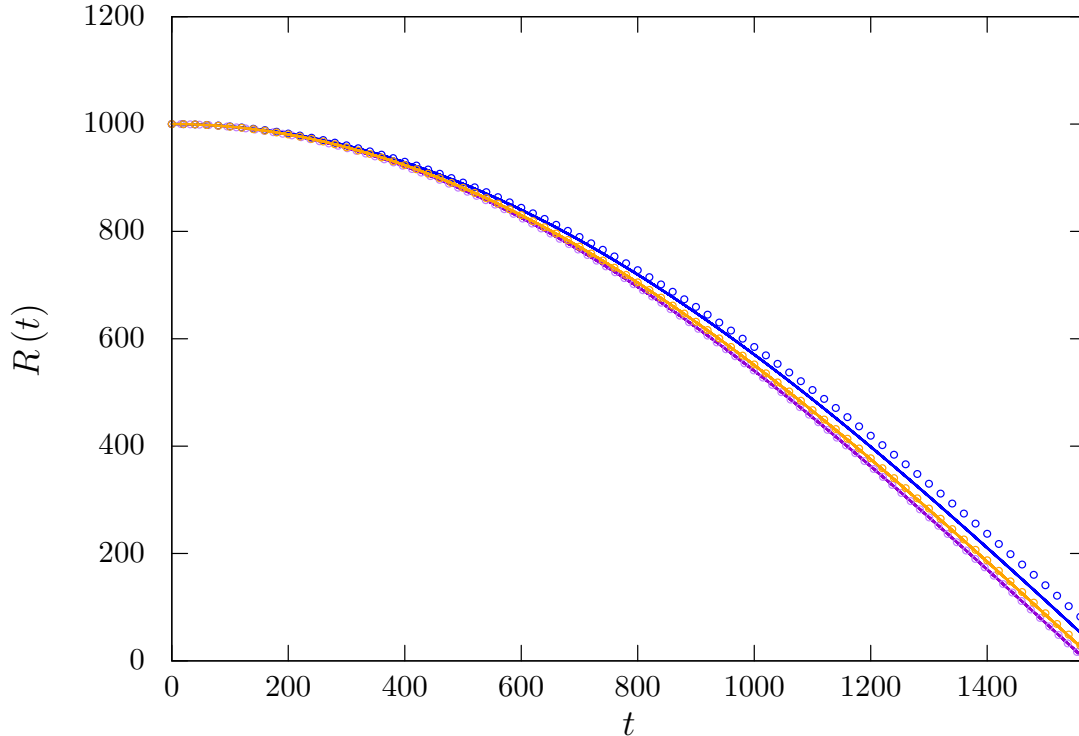


FIG. 15: Radius of the ring as a function of time for $\theta(t=0) = 0$ (purple), $\theta(t=0) = 0.2$ (orange) and $\theta(t=0) = 0.4$ (blue). The solid curves are the result of the field theory simulation, while the ones with circles correspond to the solution of the coupled equations (G5).

We show in Fig. 15 a comparison of the evolution of the collapsing ring obtained in field theory with the one predicted from our effective action described in Eq. (G1). Our results show a very good agreement between these two descriptions provided that one starts with a relatively small value of the amplitude of the shape mode. For larger values one can not neglect the presence of radiation and the ring trajectory starts to deviate from the effective action prediction.

-
- [1] H. Arodz, Acta Phys. Polon. **B22**, 511 (1991).
 - [2] M. Goodband and M. Hindmarsh, Phys. Rev. **D52**, 4621 (1995).
 - [3] A. Alonso-Izquierdo, W. Garcia Fuertes, and J. Mateos Guilarte, Phys. Lett. **B753**, 29 (2016), 1509.06632.
 - [4] J. J. Blanco-Pillado, D. Jiménez-Aguilar, and J. Urrestilla, JCAP **01**, 027 (2021), 2006.13255.
 - [5] J. J. Blanco-Pillado, D. Jiménez-Aguilar, J. M. Queiruga, and J. Urrestilla, JCAP **10**, 047 (2021), 2107.02215.

- [6] Y. Nambu, pp 269-78 of *Symmetries and Quark Models*. /Chand, Ramesh (ed.). New York Gordon and Breach, Science Publishers, Inc. (1970), URL <https://www.osti.gov/biblio/4118139>.
- [7] T. Goto, *Prog. Theor. Phys.* **46**, 1560 (1971).
- [8] H. Nielsen and P. Olesen, *Nuclear Physics B* **61**, 45 (1973).
- [9] T. W. B. Kibble, *J. Phys.* **A9**, 1387 (1976).
- [10] R. Jeannerot, J. Rocher, and M. Sakellariadou, *Phys. Rev. D* **68**, 103514 (2003), hep-ph/0308134.
- [11] K. D. Olum and J. J. Blanco-Pillado, *Phys. Rev. D* **60**, 023503 (1999), gr-qc/9812040.
- [12] K. D. Olum and J. J. Blanco-Pillado, *Phys. Rev. Lett.* **84**, 4288 (2000), astro-ph/9910354.
- [13] J. J. Blanco-Pillado and K. D. Olum, *Phys. Rev. D* **96**, 104046 (2017), 1709.02693.
- [14] P. Auclair et al., *JCAP* **04**, 034 (2020), 1909.00819.
- [15] M. Hindmarsh, J. Lizarraga, J. Urrestilla, D. Daverio, and M. Kunz, *Phys. Rev. D* **96**, 023525 (2017), 1703.06696.
- [16] M. Hindmarsh, J. Lizarraga, A. Urrio, and J. Urrestilla, *Phys. Rev. D* **104**, 043519 (2021), 2103.16248.
- [17] T. Vachaspati, *Kinks and domain walls: An introduction to classical and quantum solitons* (Cambridge University Press, 2010), ISBN 978-0-521-14191-8, 978-0-521-83605-0, 978-0-511-24290-8.
- [18] R. Rajaraman, *Solitons and Instantons. An introduction to solitons and instantons in Quantum Field Theory* (1982).
- [19] Vachaspati and T. Vachaspati, *Phys. Lett. B* **238**, 41 (1990).
- [20] N. S. Manton and H. Merabet, *Nonlinearity* **10**, 3 (1997), hep-th/9605038.
- [21] A. Vilenkin and E. S. Shellard, *Cosmic Strings and Other Topological Defects* (Cambridge University Press, 2000), ISBN 978-0-521-65476-0.
- [22] K.-i. Maeda and N. Turok, *Phys. Lett. B* **202**, 376 (1988).
- [23] R. Gregory, D. Haws, and D. Garfinkle, *Phys. Rev. D* **42**, 343 (1990).
- [24] R. Gregory, *Phys. Rev. D* **43**, 520 (1991).
- [25] M. R. Anderson, F. Bonjour, R. Gregory, and J. Stewart, *Phys. Rev. D* **56**, 8014 (1997), hep-ph/9707324.
- [26] E. Witten, *Nucl. Phys. B* **249**, 557 (1985).
- [27] R. L. Davis and E. P. S. Shellard, *Nucl. Phys. B* **323**, 209 (1989).
- [28] L. Rayleigh, *The London, Edinburgh, and Dublin Philosophical Magazine and Journal of Science* **24**, 145 (1887).
- [29] I. Kovacic, R. Rand, and S. Mohamed Sah, *Applied Mechanics Reviews* **70** (2018).

- [30] E. Mettler, in *Dynamic Stability of Structures*, edited by G. Herrmann (Pergamon, 1967), pp. 169–188, ISBN 978-1-4831-9821-7, URL <https://www.sciencedirect.com/science/article/pii/B9781483198217500156>.
- [31] A. Saurabh, T. Vachaspati, and L. Pogosian, *Phys. Rev. D* **101**, 083522 (2020), 2001.01030.
- [32] G. Mur, *IEEE Transactions on Electromagnetic Compatibility* **EMC-23**, 377 (1981).